

# HYDRODYNAMICS OF FLUIDIZATION IN AN ANNULAR SPACE

by

**L.M. Wanicka**

A dissertation submitted in partial fulfilment of the requirements for the degree  
Master of Engineering in Chemical Engineering

Department of Chemical Engineering  
Faculty of Engineering, Built Environment and Information Technology

University of Pretoria  
Pretoria  
South Africa

December 2015

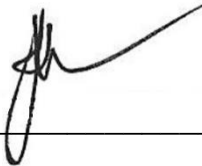
**Supervisor: Professor M.D. Heydenrych**



# DECLARATION

I, Lucja Michalina Wanicka, hereby declare that this Master's dissertation is my own original work. I have not copied from any other student's work or from any other sources except where due reference or acknowledgement is made explicitly in the text, nor has any part been written for me by another person.

It is the intention that this Masters dissertation be submitted for the degree of Master of Engineering in Chemical Engineering at the University of Pretoria. Therefore I further declare that this dissertation has not been submitted to any other educational institution for any examination, diploma, degree or other form of qualification.



---

Lucja M Wanicka

8 December 2015

# PUBLICATIONS AND PRESENTATIONS

**Some of the results presented in this dissertation have been published in:**

Wanicka, LM and Heydenrych, MD (2014) “Hydrodynamics of fluidization in an annular space”, *South African Journal of Chemical Engineering*, 19(3), 82 – 89.

Wanicka, LM and Heydenrych, MD (2014) “Hydrodynamics of fluidization in an annular space”, a paper published in the conference proceedings of *IFSA 2014: Industrial Fluidization South Africa*, 19 – 20 November 2014, Johannesburg, South Africa.

Wanicka, LM, Airaga, EM and Heydenrych, MD (2015) “Hydrodynamics of Fluidization in an Annular Space: A comparative study using various bed materials and gas distributor designs”, a paper published in *Proceedings of 44<sup>th</sup> The IIER International Conference*, 1 November 2015, Cape Town, South Africa, 8 – 12.

**And presented at:**

The 5<sup>th</sup> Conference on Industrial Fluidization, South Africa, IFSA 2014.

# HYDRODYNAMICS OF FLUIDIZATION IN AN ANNULAR SPACE

## SYNOPSIS

The present investigation was aimed at studying the hydrodynamic behaviour of fluidization in an unconventional fluidized bed geometry consisting of a vertically orientated annular space. It was hypothesized that by using multiple gas injectors, orientated tangentially to the annulus walls, induced rotating fluid bed behaviour would occur in the annulus. Annular fluidized beds with induced rotating fluid bed behaviour would ensure complete lateral mixing of solids and gas-solids, and offer the additional advantage that the feed inlet to the fluidized bed can be positioned at a single location.

A physical model, constructed of two Perspex tubes, was used to study the behaviour of a fluidized bed in an annulus with various bed materials and gas distributor designs. In order to study the hydrodynamics of the annular fluidized bed in more detail, representative 2-dimensional computational fluid dynamic (CFD) models were also simulated.

In experiments conducted with multiple tangential air injectors, induced rotating fluid bed behaviour was not observed throughout the entire range of superficial gas velocities tested with any bed material in the annulus. Induced rotating fluid bed behaviour was not observed even after a reduction in the air injector diameter and the addition of a secondary blower. It was concluded that the centrifugal forces were significantly less than initially anticipated with this air distributor design. In addition, it was also concluded that regions of stationary bed material located directly behind

the air injectors significantly impeded the momentum transfer between the moving air and bed material, preventing any bed rotation in the annulus.

In the experiments conducted using the overlapping metal leaves air distributor design, stationary regions of bed material were also observed on top of the overlapping metal leaves. These regions were significantly smaller than the regions observed directly behind the tangential air injectors. Unfortunately, induced rotating fluid bed behaviour was not observed with any of the bed materials throughout the entire range of superficial gas velocities tested. It was therefore concluded that the vertical and tangential components ( $v\sin\theta$  and  $v\cos\theta$ ) of the air velocity flowing through the overlapping metal leaves were insufficient to result in uniform fluidization or the desired induced rotating bed behaviour in the annulus.

In order to overcome the problems experienced with the overlapping metal leaves air distributor design, a new air distributor was designed and printed 3-dimensionally to have double the number of slits for the fluidizing air to flow out of. Although induced rotating fluid bed behaviour was once again not observed, uniform bubbling fluidization was apparent during experiments conducted with river sand and poppy seeds as the bed material in the annulus. This observation implied that the vertical component ( $v\sin\theta$ ) of the air velocity flowing through the slits was sufficient to achieve uniform fluidization in the annulus, significantly increasing the mixing effects of the bed material. However, the tangential component ( $v\cos\theta$ ) of the velocity was still insufficient to induce any rotation of the fluid bed.

Based on the sensitivity studies performed, a minimum percentage open area of 1.6% was recommended to ensure uniform fluidization of the bed material in the annulus. It was hypothesized that once uniform fluidization is achieved, induced rotating fluid bed behaviour is likely to occur with sufficient fluidizing air flowing in the tangential direction, since a uniformly fluidized bed experiences little resistance to flow and/or movement. In order to test this hypothesis, it was recommended that

future experiments should be conducted using slit (or hole) angles below  $45^\circ$  and with blowers able to achieve higher superficial gas velocities ( $> 1$  m/s) in the annulus.

The Euler-Euler Model – Laminar Flow Interface in COMSOL Multiphysics® software was used to study the hydrodynamic behaviour of the annular fluidized bed in more detail. The simulation results proved beneficial since the CFD models could illustrate several hydrodynamic properties not visibly obvious in the experiments conducted with the Perspex model. However, it is recommended that more accurate CFD models of the annular fluidized bed should be developed that model the dispersed phase as a particle size distribution and model the annulus in 3D, and that a turbulent CFD model, capable of simulating high Reynolds numbers, be used. Such a CFD model can then be used to test porous plate-type distributors and variations in slit or hole angles with high superficial gas velocities in the annulus, as previously recommended.

If induced rotating fluid bed behaviour is successfully modelled using CFD, the model can then be used to check whether sufficient contact time is available for the pyrolysis reactions to occur at the recommended higher superficial gas velocities. If not, the design concept of having an induced rotating fluid bed in the annular pyrolysis chamber of the new fluidized bed fast pyrolyser could be impractical, and in such an event, a rotating gas distributor plate should be considered instead.

**KEYWORDS:** hydrodynamic, fluidization, annulus, computational fluid dynamics

# ACKNOWLEDGEMENTS

I would like to thank everyone who contributed in some way to the work described in this dissertation. First and foremost, I would like to thank my academic supervisor, Professor Mike Heydenrych, for his thoughtful guidance and useful suggestions. I would also like thank the Paper Manufacturers Association of South Africa (PAMSA) and Sappi Southern Africa Ltd for their support and funding of this research project. Lastly, and most importantly, special thanks to my family, friends and colleagues who have continually supported and encouraged me throughout the duration of my studies.

# TABLE OF CONTENTS

|  |             |
|--|-------------|
| <b>Declaration</b> .....                     | <b>i</b>    |
| <b>Publications and Presentations</b> .....  | <b>ii</b>   |
| <b>Synopsis</b> .....                        | <b>iii</b>  |
| <b>Acknowledgements</b> .....                | <b>vi</b>   |
| <b>List of Figures</b> .....                 | <b>x</b>    |
| <b>List of Tables</b> .....                  | <b>xiii</b> |
| <b>List of Abbreviations</b> .....           | <b>xiv</b>  |
| <b>Nomenclature</b> .....                    | <b>xv</b>   |
| <br>   |             |
| <b>Chapter 1: Introduction</b> .....         | <b>1-1</b>  |
| 1.1 Background.....                          | 1-1         |
| 1.2 Objective of Investigation.....          | 1-1         |
| 1.3 Method.....                              | 1-1         |
| 1.4 Application of Research.....             | 1-2         |
| 1.5 Structure of Dissertation.....           | 1-2         |
| 1.6 Reference.....                           | 1-3         |
| <br>   |             |
| <b>Chapter 2: Literature Review</b> .....    | <b>2-1</b>  |
| 2.1 Fundamentals of Fluidization.....        | 2-1         |
| 2.1.1 Classification of Particles.....       | 2-4         |
| 2.1.2 Elutriation and Entrainment.....       | 2-5         |
| 2.1.3 Attrition.....                         | 2-6         |
| 2.2 Experimental Measurement Techniques..... | 2-6         |
| 2.3 Designing of Fluidized Bed Systems.....  | 2-7         |
| 2.4 Unconventional Fluidized Beds.....       | 2-11        |



|  |            |
|--|------------|
| 2.5 Fluidized Bed Modelling .....              | 2-13       |
| 2.6 References.....                            | 2-15       |
| <b>Chapter 3: Materials &amp; Methods.....</b> | <b>3-1</b> |
| 3.1 River Sand.....                            | 3-1        |
| 3.2 Additional Materials .....                 | 3-3        |
| 3.3 Pressure Drop Measurements .....           | 3-6        |
| <b>Chapter 4: Tangential Injectors .....</b>   | <b>4-1</b> |
| 4.1 Design Concept .....                       | 4-1        |
| 4.2 Construction.....                          | 4-2        |
| 4.3 Initial Experiments.....                   | 4-3        |
| 4.4 Results and Discussion .....               | 4-6        |
| 4.5 Alterations .....                          | 4-8        |
| 4.5.1 Reducing the Air Injector Diameter ..... | 4-9        |
| 4.5.2 Installing an Additional Blower.....     | 4-10       |
| 4.5.3 Testing of Additional Materials .....    | 4-11       |
| 4.6 Conclusions and Recommendations .....      | 4-15       |
| <b>Chapter 5: Angled Blades.....</b>           | <b>5-1</b> |
| 5.1 Design Concept .....                       | 5-1        |
| 5.2 Construction.....                          | 5-1        |
| 5.3 Initial Experiments.....                   | 5-3        |
| 5.4 Results and Discussion .....               | 5-5        |
| 5.5 Alterations .....                          | 5-8        |
| 5.5.1 Increasing the Number of Slits.....      | 5-8        |
| 5.5.2 Independent Research.....                | 5-11       |
| 5.5.3 Dimensional Analysis.....                | 5-13       |
| 5.6 Conclusions and Recommendations .....      | 5-17       |
| 5.7 Reference .....                            | 5-19       |

|  |            |
|--|------------|
| <b>Chapter 6: CFD Simulations .....</b>                  | <b>6-1</b> |
| 6.1 The Euler-Euler Model .....                          | 6-1        |
| 6.2 Tangential Injectors.....                            | 6-2        |
| 6.2.1 River Sand.....                                    | 6-4        |
| 6.2.2 Additional Materials .....                         | 6-7        |
| 6.3 Angled Blades.....                                   | 6-9        |
| 6.3.1 River Sand.....                                    | 6-9        |
| 6.3.2 Poppy Seeds.....                                   | 6-12       |
| 6.4 Limitations of CFD Results.....                      | 6-13       |
| 6.5 Conclusions and Recommendations .....                | 6-14       |
| 6.6 Reference .....                                      | 6-15       |
| <br>   |            |
| <b>Chapter 7: Conclusions &amp; Recommendations.....</b> | <b>7-1</b> |
| 7.1 Perspex Model Conclusions .....                      | 7-1        |
| 7.1.1 Tangential Injectors.....                          | 7-1        |
| 7.1.2 Angled Blades.....                                 | 7-2        |
| 7.2 Conclusions of CFD Simulations .....                 | 7-3        |
| 7.3 Recommendations for Future Work .....                | 7-4        |

# LIST OF FIGURES

|   |      |
|---|------|
| <b>Figure 2-1:</b> Gas-solid fluidization regimes (adapted from Kunii and Levenspiel (1991: 2)) .....                                       | 2-2  |
| <b>Figure 2-2:</b> Geldart’s powder classification diagram (Geldart, 1973) .....  | 2-4  |
| <b>Figure 2-3:</b> Zones in a fluidized bed (Rhodes, 2008: 184) .....   | 2-5  |
| <b>Figure 2-4:</b> Schematic diagram of fluidized bed system development (adapted from Jiang <i>et al.</i> (2003: 326)) .....               | 2-10 |
| <b>Figure 2-5:</b> TORBED reactor (Torftech, sa) .....  | 2-13 |
| <b>Figure 2-6:</b> Fixed angled blades used as the distributor in the TORBED reactor (Sreenivasan & Raghavan, 2002) .....                   | 2-13 |
| <br>  |      |
| <b>Figure 3-1:</b> Particle size distribution of river sand .....   | 3-2  |
| <b>Figure 3-2:</b> SEM images of river sand .....   | 3-2  |
| <b>Figure 3-3:</b> Particle size distribution of the ilmenite and the ilmenite-sand mixture .....   | 3-3  |
| <b>Figure 3-4:</b> SEM images of ilmenite-sand mixture .....  | 3-4  |
| <b>Figure 3-5:</b> SEM images of mustard seeds .....  | 3-5  |
| <b>Figure 3-6:</b> SEM images of poppy seeds .....  | 3-5  |
| <b>Figure 3-7:</b> Schematic diagram of air flow from double-stage side-channel blower to tapped holes in rolled stainless steel pipe ..... | 3-6  |
| <b>Figure 3-8:</b> Detailed diagram of designed orifice plate (measurements not to scale) .....   | 3-7  |
| <br>  |      |
| <b>Figure 4-1:</b> Clockwise rotation of the fluid bed in an annular space .....  | 4-1  |
| <b>Figure 4-2:</b> Detailed diagram of the air injector housings with copper pipes .....  | 4-2  |
| <b>Figure 4-3:</b> Photograph of the assembled Perspex model .....  | 4-3  |

**Figure 4-4:** (*Left*) Bed material removed at several air injectors (2.0 kg river sand); (*right*) accumulation of bed material at other air injectors (2.0 kg river sand) .....4-4

**Figure 4-5:** Pressure along the length of the rolled pipe as a function of the volumetric flow rate of the air.....4-5

**Figure 4-6:** Comparison of bed expansion of river sand from static bed height as a function of superficial gas velocity .....4-6

**Figure 4-7:** Instantaneous snapshots of jet formation (3.5 kg river sand) .....4-8

**Figure 4-8:** (*Left*) Depletion of bed material at several air injectors (3.0 kg ilmenite-sand mixture); (*right*) turbulent fluidization(4.0 kg ilmenite-sand mixture)..... 4-11

**Figure 4-9:** Spouted fluidized bed behaviour (1.5 kg mustard seeds)..... 4-12

**Figure 4-10:** Comparison of bed expansion of poppy seeds from static bed height as a function of superficial gas velocity ..... 4-13

**Figure 4-11:** (*Top*) Jet formation (1.0 kg poppy seeds); (*bottom*) turbulent fluidization (2.0 kg poppy seeds) ..... 4-15

**Figure 5-1:** Detailed diagram of metal air distributor with overlapping metal leaves and adjustable screws.....5-2

**Figure 5-2:** Photograph of the metal air distributor.....5-3

**Figure 5-3:** Seepage of fluidizing air along the inner walls of the Perspex tubes (0.5 kg mustard seeds) .....5-5

**Figure 5-4:** Turbulent fluidization behaviour (0.5 kg poppy seeds).....5-7

**Figure 5-5:** Detailed diagram of 3D printed PLA air distributor .....5-9

**Figure 5-6:** Bubbling fluidization behaviour (0.5 kg poppy seeds) ..... 5-10

**Figure 5-7:** Viscosity for various bed materials as a function of superficial gas velocity (adapted from Airaga, 2015) ..... 5-12

**Figure 5-8:** Superficial gas velocity in annulus required to achieve uniform bubbling fluidization as a function of the slit angle (slit dimensions: 13 mm x 0.5 mm, 64 slits)..... 5-16

**Figure 6-1:** Geometry of the CFD models of the tangential injectors .....6-3

**Figure 6-2:** Instantaneous snapshots of simulation results (2.5 kg river sand; 6.5 mm tangential injectors) .....6-5

**Figure 6-3:** Dynamic viscosity of dispersed phase – encircled areas indicate areas of high dynamic viscosity (2.5 kg river sand; 6.5 mm tangential injectors) .....6-6

**Figure 6-4:** Instantaneous snapshots of simulation results (1.0 kg poppy seeds; 5 mm tangential air injectors) .....6-8

**Figure 6-5:** Instantaneous snapshots of simulation results (2.5 kg river sand; overlapping metal leaves) ..... 6-10

**Figure 6-6:** Velocity profile of continuous phase represented by proportional vectors at 1.5 seconds (2.5 kg river sand; overlapping metal leaves) ..... 6-11

**Figure 6-7:** Instantaneous snapshot of simulation results (1.0 kg poppy seeds; 3D printed air distributor with 45° slits) ..... 6-13

# LIST OF TABLES

|   |      |
|---|------|
| <b>Table 2-1:</b> Summary of key hydrodynamic characteristics of the various gas-solid fluidization regimes (adapted from Paudel, 2011).....            | 2-3  |
| <b>Table 2-2:</b> Non-intrusive measurement techniques (adapted from Silva <i>et al.</i> , 2012: 42) .....  | 2-8  |
| <b>Table 2-3:</b> Intrusive measurement techniques (adapted from Silva <i>et al.</i> , 2012: 43).....   | 2-9  |
| <b>Table 3-1:</b> Summary of characteristics of materials used in experiments.....  | 3-7  |
| <b>Table 4-1:</b> Dimensions and specifications of parts used in the Perspex model setup .....  | 4-3  |
| <b>Table 4-2:</b> Summary of river sand experimental results.....   | 4-7  |
| <b>Table 4-3:</b> Influence of the air injector diameter on the momentum transfer at a constant superficial gas velocity of 0.5 m/s in the annulus..... | 4-10 |
| <b>Table 4-4:</b> Summary of poppy seed experimental results .....  | 4-14 |
| <b>Table 5-1:</b> Dimensions and specifications of the metal air distributor.....   | 5-2  |
| <b>Table 5-2:</b> Comparison of cross-sectional areas using various air injectors at a constant superficial gas velocity of 0.5 m/s in the annulus..... | 5-4  |
| <b>Table 5-3:</b> Comparison of slit and hole dimensions and numbers to achieve a percentage open area of at least 1.6%.....                            | 5-14 |
| <b>Table 6-1:</b> Parameters for the CFD models of the tangential injectors.....  | 6-4  |
| <b>Table 6-2:</b> Material-specific parameters used in the 2.5 kg river sand loading simulation .....   | 6-4  |
| <b>Table 6-3:</b> Summary of models suitable for turbulent CFD modelling (adapted from Silva, Jiménez & Salazar, 2012: 45).....                         | 6-16 |

# LIST OF ABBREVIATIONS

|     |                                      |
|-----|--------------------------------------|
| CFD | Computational fluid dynamics         |
| CTD | Contact time distribution            |
| IMT | Intrusive measurement techniques     |
| NMT | Non-intrusive measurement techniques |
| PLA | Polylactic acid                      |
| RTD | Residence time distribution          |
| SEM | Scanning electron microscope         |
| TDH | Transport disengagement height       |

# NOMENCLATURE

## Roman symbols

|                 |  |                            |
|-----------------|--|----------------------------|
| $C_{drag}$      | Drag coefficient for a single dispersed particle   |                            |
| $d$             | Dispersed phase particle diameter  | m                          |
| $d_{sv}$        | Mean particle size   | $\mu\text{m}$              |
| $DV_{10}$       | Particle size below which 10% of the volume particles exist                                  | $\mu\text{m}$              |
| $DV_{50}$       | Particle size below which 50% of the volume particles exist;<br>volume average particle size | $\mu\text{m}$              |
| $DV_{90}$       | Particle size below which 90% of the volume particles exist                                  | $\mu\text{m}$              |
| $F$             | Interphase momentum transfer   | $\text{N}/\text{m}^3$      |
| $g$             | Acceleration due to gravity  | $9.8 \text{ m}/\text{s}^2$ |
| $L_f$           | Bed height at bubbling fluidization  | m                          |
| $L_m$           | Static bed height  | m                          |
| $L_{mf}$        | Bed height at minimum fluidization   | m                          |
| $p_s$           | Solid pressure   | Pa                         |
| $q$             | Dynamic pressure   | Pa                         |
| $u$             | Velocity of phase  | $\text{m}/\text{s}$        |
| $u_f$           | Bubbling fluidization velocity   | $\text{m}/\text{s}$        |
| $u_{mf}$        | Minimum fluidization velocity  | $\text{m}/\text{s}$        |
| $u_{transport}$ | Fluidization velocity where transport of bed material occurs                                 | $\text{m}/\text{s}$        |
| $v$             | Velocity of fluidizing medium  | $\text{m}/\text{s}$        |

## Greek symbols

|                    |                                  |
|--------------------|----------------------------------|
| $\beta$            | Drag force coefficient           |
| $\varepsilon_{mf}$ | Porosity at minimum fluidization |



|             |                              |                          |
|-------------|------------------------------|--------------------------|
| $\varphi$   | Phase volume fraction        |                          |
| $\emptyset$ | Sphericity of a particle     |                          |
| $\rho$      | Density of fluidizing medium | $\text{kg/m}^3$          |
| $\rho_b$    | Bulk density of particles    | $\text{kg/m}^3$          |
| $\rho_s$    | Density of particle          | $\text{kg/m}^3$          |
| $\mu$       | Dynamic viscosity            | $\text{Pa}\cdot\text{s}$ |

### Subscripts

|     |   |
|-----|---|
| $c$ | Quantities relating to the continuous phase |
| $d$ | Quantities relating to the dispersed phase  |

---

# CHAPTER 1: INTRODUCTION

---

## 1.1 Background

In recent years, researchers have been experimenting with unconventional fluidized bed geometries in order to overcome typical problems experienced in conventional fluidized beds such as inadequate lateral mixing of solids and gas-solids, attrition and bed material loss from elutriation and entrainment (Yang, 2003: 562). In order to overcome these shortcomings, conventional fluidized beds used in industrial applications were modified, resulting in unconventional fluidized beds.

## 1.2 Objective of Investigation

The present investigation was aimed at studying the hydrodynamic behaviour of fluidization in an unconventional fluidized bed geometry consisting of a vertically orientated annular space. It was hypothesized that by using multiple gas injectors orientated tangentially to the annulus walls, induced rotating fluid bed behaviour would occur in the annulus. Annular fluidized beds with induced rotating fluid bed behaviour would ensure complete lateral mixing of solids and gas-solids, and offer the additional advantage that the feed inlet to the fluidized bed can be positioned at a single location.

## 1.3 Method

A physical model, constructed of two Perspex tubes, was used to study the behaviour of a fluidized bed in an annulus with various bed materials and gas distributor designs. In order to study the hydrodynamics of the annular fluidized bed in more

detail, representative 2-dimensional computational fluid dynamic (CFD) models were also simulated in commercially available software (COMSOL Multiphysics®).

## 1.4 Application of Research

A new fluidized bed fast pyrolyser is being developed at the Pyrolysis Laboratory at the Department of Chemical Engineering of the University of Pretoria. The pyrolyser is annular in design, with the pyrolysis chamber being a narrow annulus located on the outer circumference of the combustion chamber. The present investigation was carried out to check the validity of the design concept, in which the fluidized bed in the pyrolysis chamber experiences induced rotating fluid bed behaviour.

## 1.5 Structure of Dissertation

The present dissertation is structured according to the following chapters:

- **Chapter 2** – reviews the literature, including the fundamentals of fluidization, designing of fluidized bed systems, unconventional fluidized beds as well as fluidization bed modelling.
- **Chapter 3** – describes the characteristics of the various bed materials tested, illustrates how the fluidizing air flows into the annulus and how the pressure drop measurements were obtained.
- **Chapter 4** – describes the design, construction and experiments conducted using multiple air injectors orientated tangentially to the outer walls of the annulus.
- **Chapter 5** – describes the design, construction and experiments conducted using two different air distributor designs – one being a metal air distributor constructed of multiple overlapping metal leaves, and the other being a 3D printed air distributor with multiple angled slits.

- **Chapter 6** – discusses and illustrates the CFD simulation results.
- **Chapter 7** – summarises the conclusions and recommendations drawn up in Chapters 4, 5 and 6.

## 1.6 Reference

Yang, W (2003) *Other Nonconventional Fluidized Beds*, In Yang, W (ed) *Handbook of Fluidization and Fluid-Particle Systems*, Marcel Dekker Inc, United States of America.

---

# CHAPTER 2: LITERATURE REVIEW

---

Fluidized bed technology has been applied to a large variety of processes, including drying, the combustion of coal and fluid catalytic cracking and reforming (Pell, Dunson & Knowlton, 2007: 17-2). Fluidized beds are preferred to fixed bed reactors as they offer good particle mixing, good temperature control and adaptability to high-pressure and high-temperature operations (Jiang, Wei & Fan, 2003: 326). In addition, fluidized beds are also suitable for large-scale operations due to their simple geometric designs (Jiang *et al.*, 2003: 326).

## 2.1 Fundamentals of Fluidization

Fluidization occurs when a packed bed of solid particles is transformed into a fluid-like state by means of suspension by a gas or liquid. The suspended bed of particles behaves similarly to a fluid – seeking its own level and causing large, heavy objects to sink (Pell *et al.*, 2007: 17-2). Depending on the superficial gas velocity passed through the bed of particles, a fluidized bed can operate in various regimes, as illustrated in Figure 2-1. In the fixed bed regime, the superficial gas velocity is sufficiently low that it only percolates through the void spaces between the particles (Kunii & Levenspiel, 1991: 1). The height of the bed remains constant at the static bed height,  $L_m$ .

As the superficial gas velocity increases, the particles become suspended in the upward-flowing gas, and the height of the bed increases to the bed height at minimum fluidization,  $L_{mf}$ . At minimum fluidization, the frictional force between the particles and gas is sufficient to counter-balance the mass of the bed of particles and the bed is said to be “just fluidized” (Kunii & Levenspiel, 1991: 1). The

superficial gas velocity at which the bed becomes a fluidized bed is referred to as the minimum fluidization velocity,  $u_{mf}$ . This velocity can also be calculated using Equation 2-1, where  $\phi$  denotes the sphericity of the particles;  $d$  denotes the average particle size;  $\mu$  is the viscosity of the bed of particles;  $g$  is the acceleration due to gravity;  $\rho_s$  is the particle density;  $\rho$  is the density of the fluidizing medium; and  $\epsilon_{mf}$  is the porosity of the bed at minimum fluidization.

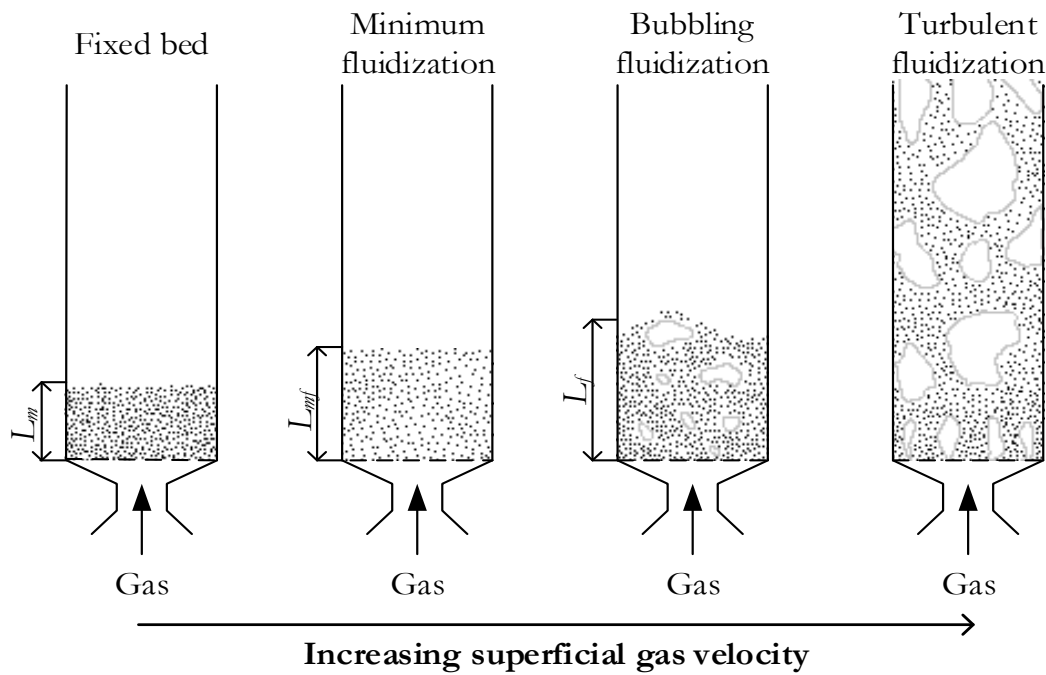


**Figure 2-1:** Gas-solid fluidization regimes (adapted from Kunii and Levenspiel (1991: 2))

$$u_{mf} = \frac{(\phi d)^2}{150\mu} [g(\rho_s - \rho)] \frac{\epsilon_{mf}^3}{1 - \epsilon_{mf}} \quad (2-1)$$

With a further increase in superficial gas velocity ( $u_f$ ), bubbles of the upward-flowing gas form in the bed, resulting in vigorous particle movement. The height of the bubbling fluidized bed,  $L_f$ , is only slightly greater than the height of the bed at minimum fluidization. When the superficial gas velocity is increased even further, the fluidized bed begins to operate in the turbulent fluidization regime. In this regime, bubbles are no longer formed, and instead solid clusters of particles and

voids of gas of various sizes travel up through the bed (Kunii & Levenspiel, 1991: 3). With an even further increase in the superficial gas velocity ( $u_{transport}$ ), the bed material can be completely removed from the fluidized bed, resulting in phenomena referred to as fast fluidization and pneumatic conveying. Table 2-1 summarises key hydrodynamic characteristics of these various gas-solid fluidization regimes.

**Table 2-1:** Summary of key hydrodynamic characteristics of the various gas-solid fluidization regimes (adapted from Paudel, 2011)

| <b>Fluidization regime</b>    | <b>Velocity range</b>     | <b>Description of characteristics</b>  |
|-------------------------------|---------------------------|--|
| <b>Fixed bed</b>              | $0 \leq u < u_{mf}$       | Superficial gas velocity is low; gas only percolates through void spaces between particles of the bed material; no bed expansion.              |
| <b>Minimum fluidization</b>   | $u = u_{mf}$              | Bed material particles are suspended; the bed begins to expand; bed surface is well defined.   |
| <b>Bubbling fluidization</b>  | $u_{mf} < u \leq u_f$     | Bubble formation resulting in vigorous particle movement; bed expansion only slightly greater than the bed height at minimum fluidization.     |
| <b>Turbulent fluidization</b> | $u_f < u < u_{transport}$ | Bubbles are no longer formed; solid clusters of particles and voids of gas of various sizes observed; bed surface is difficult to distinguish. |
| <b>Fast fluidization</b>      | $u \geq u_{transport}$    | Dilute and dense areas coexist; dense regions along the walls, moving downwards; main part of suspension moves upwards.                        |
| <b>Pneumatic conveying</b>    | $u \geq u_{transport}$    | Typically a once-through operation; disappearance of dense regions; vertically uniform particle distribution.                                  |

### 2.1.1 Classification of Particles

The ease with which particles can be fluidized by a gas is dependent on the intrinsic properties of the particles such as their size, shape, density and morphology. Generally, fine low-density particles are fluidized more evenly than large dense ones, on condition that the particles are not so small that the London-van der Waals attractive forces cause the particles to stick together (Richardson, Harker & Backhurst, 2002: 317). Powders that contain a large size distribution will usually fluidize more evenly than those of a uniform size since the fine particles coat the larger ones with a “lubricating layer” (Richardson *et al.*, 2002: 317). The sphericity of the particles ( $\phi$ ), defined as the degree to which the particles resemble a sphere, also affects the ease of fluidization of the powder as spherical particles tend to fluidize more evenly (Richardson *et al.*, 2002: 317). Based on experimental observations of different powders, Geldart (1973) classified the behaviour of solid particles fluidized by gases into four distinct groups, as illustrated in Figure 2-2.

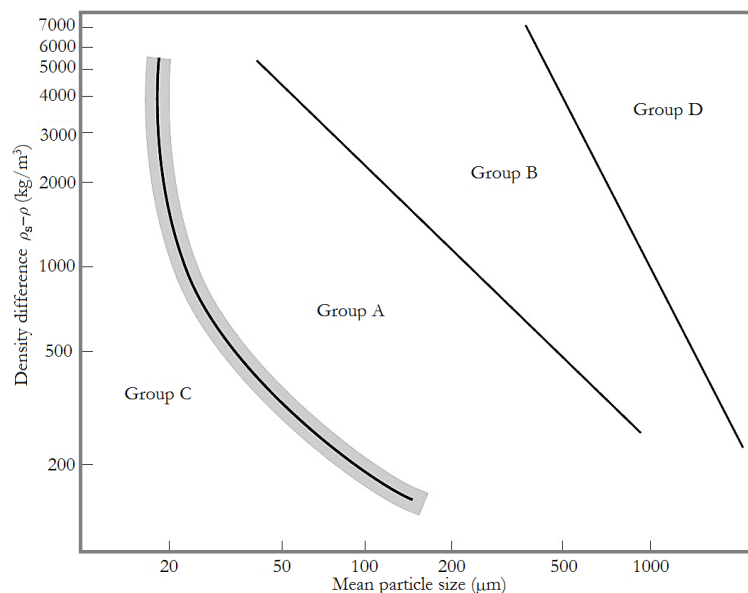


**Figure 2-2:** Geldart’s powder classification diagram (Geldart, 1973)

The four groups are characterised by the density difference between the particles and the fluidizing medium, and by the mean particle size ( $d_{sv}$ ) (Yang, 2003: 75).



Although other researchers in the field have systematized the various types of gas fluidization, Geldart's powder classification remains the standard most frequently used in industry.

### 2.1.2 Elutriation and Entrainment

A fluidized bed can be divided into several vertical zones, as illustrated in Figure 2-3. At the base of the fluidizing vessel is the dense fluidized bed containing the majority of the solid particles. Above this zone is the freeboard region in which the density of solids decreases with height. At relatively low superficial gas velocities, a more or less distinct upper surface separates the bed from the freeboard (Kunii & Levenspiel, 1991: 165).

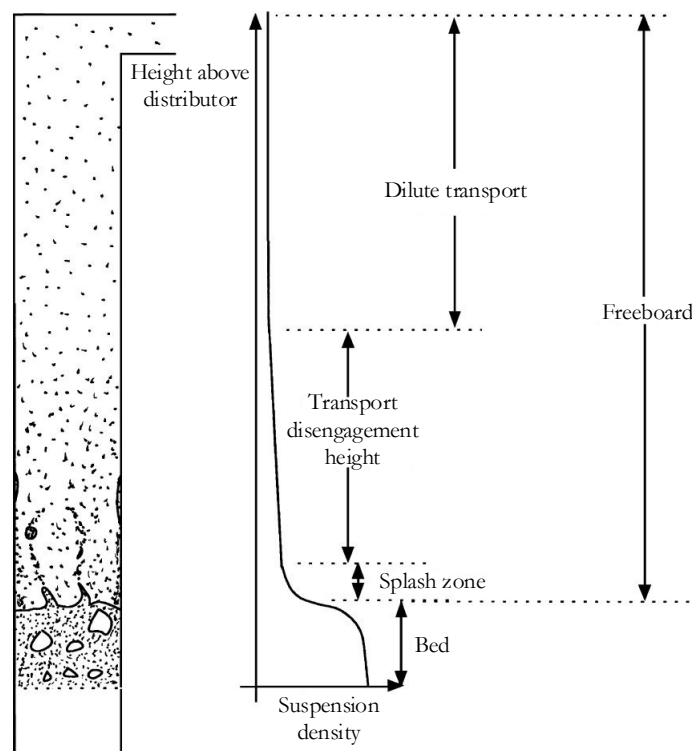


**Figure 2-3:** Zones in a fluidized bed (Rhodes, 2008: 184)

With an increase in the superficial gas velocity, a new zone characterised by a sharp decay of the solids concentration emerges between the bed and the freeboard,

referred to as the splash zone (Werther & Hartge, 2003: 134). In this zone, the distinct surface separating the bed and freeboard starts to fluctuate and increasing amounts of solids are carried out from the bed (Werther & Hartge, 2003: 134). Above the splash zone, the solids concentration gradually decays until it becomes nearly constant. The distance between the splash zone and the point at which the solids concentration becomes constant is referred to as the transport disengagement height (TDH). Above the TDH, dilute transportation of solids occurs. The flux of solids carried out of the fluidized bed by the fluidizing medium is referred to as entrainment, whereas the separation or removal of fine solids contained in the bed material is referred to as elutriation (Kunii & Levenspiel, 1991: 166).

### **2.1.3 Attrition**

The vigorous motion experienced by the bed material in a fluidized bed causes inter-particle collisions and bed-to-wall impacts, resulting in the gradual degradation of the individual bed particles (Werther & Rappenhagen, 2003: 221). This unwanted phenomenon is referred to as attrition and, depending on its severity, it may affect the performance of the fluidizing bed. Attrition alters the bed particle size distribution due to the generation of fine solids which cannot be kept inside the system. As these fine solids are removed from the fluidized bed, they can burden filtration and collection systems downstream (Werther & Rappenhagen, 2003: 221).

## **2.2 Experimental Measurement Techniques**

In order to better understand the hydrodynamics of fluidized beds, researchers have developed several measurement techniques able to analyse experimental data. These experimental measurement techniques are classified as either non-intrusive measurement techniques (NMT) (Table 2-2) or intrusive measurement techniques (IMT) (Table 2-3). According to Silva, Jiménez and Salazar (2012: 41), NMTs are

more desirable as they characterise the flow within a fluidized bed and do not disturb the flow behaviour. In contrast, IMTs are generally probes used to study local basic flow phenomena and typically used only as research instruments (Silva *et al.*, 2012: 41).

## 2.3 Designing of Fluidized Bed Systems

According to Jiang *et al.* (2003: 330), many factors can affect the optimum performance of a fluidized bed system, including hydrodynamics, heat and mass transfer of inter- and intra-particles, as well as the complexities of any reaction kinetics. The design of the components, such as the fluidizing vessel, the gas distributor, cyclones, heat exchangers, the expanded section and the baffles, will also influence the performance of the fluidized bed system. A typical fluidized bed system requires a gas distributor to ensure even distribution of the fluidizing medium and support for the particles in the bed. The gas distributor should also be able to operate for extended periods of time without plugging or breaking. Many configurations of gas distributors are employed in industry; however, the only fundamental difference between the designs is the direction of the gas entry: upwards, laterally or downwards. Cyclones are usually also included in fluidized bed systems to capture and separate solid particles from the outlet gas exiting the fluidized bed. The separated solid particles are then fed back into the fluidized bed by means of a dipleg. A heat generator can also be included, which either removes generated heat or adds required heat to the fluidized bed. It can either be immersed in the bed material, placed between the bed and the freeboard, or placed along the wall as in fluidized bed coal combustors (Jiang *et al.*, 2003: 328). Expanded sections on top of fluidized beds are generally used to reduce the linear gas velocity in the freeboard region, reducing any entrainment. These sections are not always necessary and will depend on the design of the gas-solid separator and the operating conditions (Jiang *et al.*, 2003: 328).

**Table 2-2:** Non-intrusive measurement techniques (adapted from Silva *et al.*, 2012: 42)

| Technique and description  | References   |
|--|--|
| <p><b>Laser Doppler Anemometry (LDA)</b></p> <p>LDA is a technology used to measure velocities of small particles in flow. The technique is based on the measurement of laser light scattered by particles that pass through a series of interference fringes. The scattered laser light oscillates with a specific frequency that is related to the velocity of the particles.</p>  | <p>Ibsen, Solberg &amp; Hjertager (2001); Ibsen, Solberg, Hjertager &amp; Johnsson (2002); Kuan, Yang &amp; Schwarz (2007); Lu, Glass &amp; Easson (2009); Mathiesen, Solberg, Arastoopour &amp; Hjertager (1999); Werther, Hage &amp; Rudnick (1996).</p>   |
| <p><b>X-ray and <math>\gamma</math>-ray</b></p> <p>Radiographic techniques based on electromagnetic radiation such as X-rays and <math>\gamma</math>-rays. The transmission of the rays through a heterogeneous medium is accompanied by attenuation of the incident radiation, and the measurement of this attenuation provides a measure of the line integral of the local mass density distribution along the path traversed by the beam.</p> | <p>Franka &amp; Heindel (2009); Newton, Fiorentino &amp; Smith (2001); Petritsch, Reinecke and Mewes (2000); Tapp, Payton, Kemsley and Wilson (2003); Wu, Cheng, Liu &amp; Jin (2008).<br/>         Du, Warsito and Fan (2005); Kumar, Moslemian and Dudukovic (1995); Tan, Dong, Wei &amp; Shi (2007); Thatte, Ghadge, Patwardhan, Joshi &amp; Singh (2004); Veluswamy, Upadhyay, Utikar, Evans, Tade, Glenny, Roy and Pareek (2011); Wang, Yang, Senior, Raghavan &amp; Duncan (2008).</p> |
| <p><b>Radioactive Particle Tracking (RPT)</b></p> <p>This technology measures the velocity field and turbulent parameters of multiphase flow. It is based on the principal of tracking the motion of a single tracer particle as a marker of the solid phase. The tracer particle contains a radioactive element emitting <math>\gamma</math>-rays.</p>  | <p>Al-Dahhan, , Dudukovic, Bhusarapu, O'hern, Trujillo &amp; Prairie (2005); Bhusarapu, Al-Dahhan &amp; Dudukovic (2006); Fraguío, Cassanello, Dagaleesan &amp; Dudukovic (2009); Khanna, Pugsley, Tanfara &amp; Dumont (2008); Larachi, Al-Dahhan, Dudukovic &amp; Roy (2008); Vaishali, Roy, Bhusarapu, Al-Dahhan &amp; Dudukovic (2007).</p>  |

### Particle Image Velocimetry (PIV)

PIV measures whole velocity fields by taking two images shortly after each other and calculating the distance individual particles have travelled within this time. The displacement of the particle images is measured in the plane of the image and used to determine the displacement of the particles.

Van Buijtenen, van Dijk, Deen, Kuipers, Leadbeater & Parker (2011); Fu, Wang, Chen, Gu & Xu (2011); He, Deen, van Sint Annaland & Kuipers (2009); Hernández-Jiménez, Sánchez-Delgado, Gómez-García & Acosta-Iborra (2011); Kashyap & Gidaspow (2011); Laverman, Roghair, van Sint Annaland & Kuipers (2008); Sathe, Thaker, Strand & Joshi (2010).

**Table 2-3:** Intrusive measurement techniques (adapted from Silva *et al.*, 2012: 43)

| Technique and description  | Reference  |
|--|--|
| <p><b>Pitot tube</b></p> <p>A mechanical method based on the determination of momentum by means of differential pressure measurements.</p>   | Al-Hasan & Al-Qodah (2007); Bader, Findlay & Knowlton (1988); Wang & Han (1999).   |
| <p><b>Fibre optic probe</b></p> <p>This technique is commonly used as an effective tool to measure the local porosity in fluidized beds.</p>   | Fischer, Peglow & Tsotsas (2011); Link, Godlieb, Tripp, Deen, Heinrich, Kuipers, Schönherr & Peglow (2009); Meggitt (2010); Wang, Sun, Chen, Deng, Zhao & Wu (2009); Ye, Qi & Zhu (2009); Zhou, Mo, Zhao, Li & Cen (2010); Zhu, Zhu, Li & Lu (2008). |
| <p><b>Capacitance probe</b></p> <p>This technique is used to measure the local dielectric constant of the gas-solid suspension which is linked to the local volume fraction of solids.</p> | Collin, Wirth & Ströder (2008); Collin, Wirth & Ströder (2009); Demori, Ferrari, Strazza & Poesio (2010); Guo & Werther (2008); Vogt, Schreiber, Brunner & Werther (2005); Wiesendorf (2000).  |

Baffles and other internal structures are usually used in fluidized beds to enhance the breakup of bubbles, promoting gas-solid contact and reducing particle entrainment (Jiang *et al.*, 2003: 328). According to Jiang *et al.* (2003: 328), the benefits of baffles are more distinct for Geldart Group B and D type powders because the bubbles formed are larger in comparison to those formed in Geldart Group A type powders (refer to Figure 2-2 for Geldart's powder classification diagram).

Krishna (1994) and Jazayeri (1995) described the general procedure for the design of fluidized bed systems, which is similar in approach to the design of multiphase reactor systems (Figure 2-4). In order to develop a fluidized bed system, process studies and the hydrodynamic behaviour of the fluidized bed should be known prior to the designing stage.

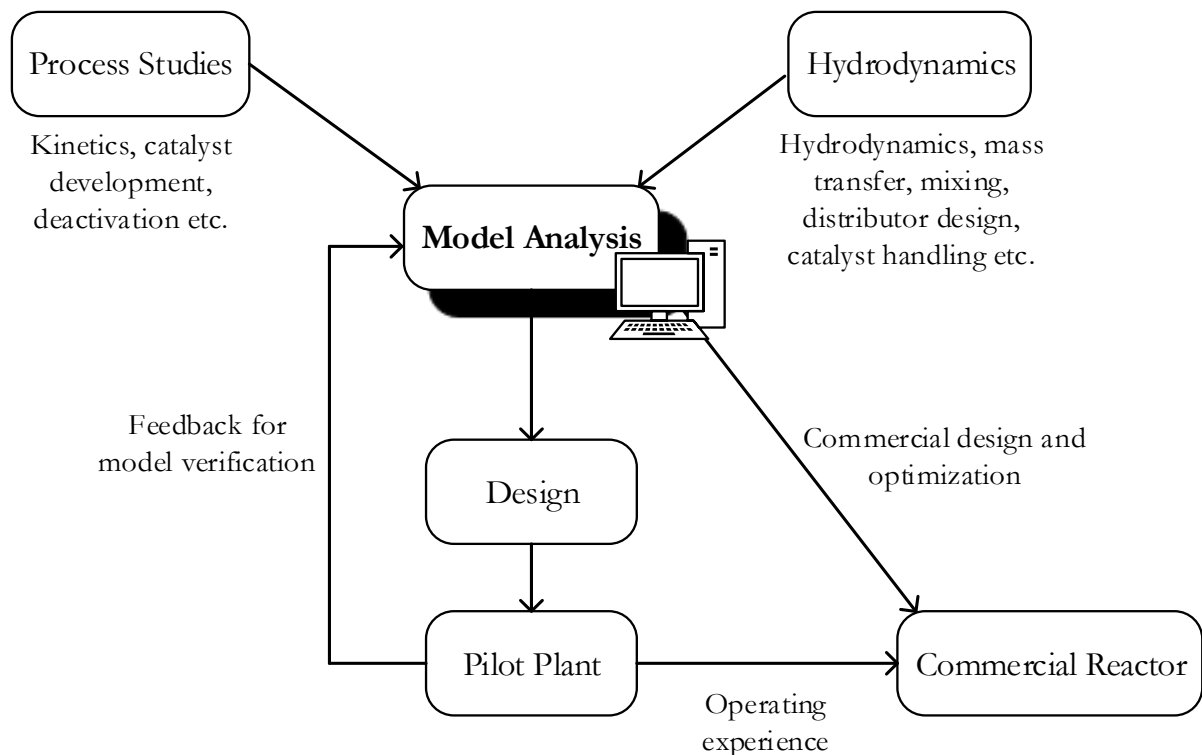


**Figure 2-4:** Schematic diagram of fluidized bed system development (adapted from Jiang *et al.* (2003: 326))

Typical process studies may include the reaction kinetics, conversion, yield, selectivity, thermodynamics as well as other process parameters that may affect any

reactions occurring inside the fluidized bed (Jiang *et al.*, 2003: 330). Hydrodynamic studies, on the other hand, can provide information on the basic flow patterns, particle attrition behaviour as well as mass and heat transfer of the fluidizing bed (Jiang *et al.*, 2003: 330).

In order to accurately predict the behaviour of a newly designed fluidized bed, it is essential that the process studies and the hydrodynamic behaviour of the fluidized bed be studied under operating conditions similar to those intended for commercial reactors. Based on the information obtained by the process studies and studies of the hydrodynamic behaviour of the fluidized bed, a model of the system can be developed and preliminary designs drawn up. A pilot unit can then be constructed to integrate the reactor with all the process-related components, including those downstream from the fluidized bed. To ensure that the gas-solid contact time and mixing patterns are similar, the pilot unit should operate in the same flow regime as the commercial unit (Jiang *et al.*, 2003: 331). The model of the system developed earlier should then be verified and modified, if necessary, to best simulate the results obtained from the pilot unit. Once the optimized design of the fluidized bed system is completed, a commercial reactor can then be developed.

## 2.4 Unconventional Fluidized Beds

In recent years, researchers have been experimenting with unconventional fluidized bed geometries in order to overcome inadequate lateral mixing of solids and gas-solids experienced in conventional fluidized beds. In addition to inadequate lateral mixing, conventional fluidized beds also experience attrition of bed material and bed material loss from elutriation and entrainment. In an attempt to mitigate these drawbacks, industrial fluidized beds are often modified, resulting in the use of unconventional fluidized beds (Yang, 2003: 562). Unconventional fluidized beds



include spouted beds, recirculating fluidized beds with draft tubes, jetting fluidized beds as well as centrifugal fluidized beds (Yang, 2003: 562).

Spouted beds, for example, are usually cylindrical vessels with fluid supplied only through a central jet nozzle located at the bottom of a conical base. Given a sufficiently high fluid velocity, the fluid stream will burst through the bed material as a spout, entraining solid particles at the spout-annulus interface (Yang, 2003: 563). Recirculating fluidized beds with draft tubes, on the other hand, appear similar to spouted beds, but because of the addition of a tubular insert (a draft tube), the operational and design characteristics are quite different. Recirculating fluidized beds with draft tubes are referred to as fluid-lift solids re-circulators, spouted fluid beds with draft tubes, internally circulating fluidized beds, or simply as circulating fluidized beds (Yang, 2003: 567). In the event that jet formation is the dominating effect in a spouted bed, this type of fluidization bed is more suitably referred to as a “jetting fluidized bed”. In such beds, the jet does not penetrate through the bed as a spouted bed, and therefore the hydrodynamic behaviour is unique (Yang, 2003: 573).

Centrifugal fluidized beds are an interesting example of unconventional fluidized beds. These fluidized beds operate on the principal that the pressure drop of the gas flowing radially inward to the bed counterbalances the centrifugal weight of the particles (Sreenivasan & Raghavan, 2002). This concept has already been applied to commercially available industrial equipment such as the “TORBED” reactor, as illustrated in Figure 2-5.

The TORBED reactor produces a toroidal mixing motion of the fluidized bed particles by injecting the fluidizing medium at the base of the reactor with the use of fixed angled blades producing a swirling motion, as illustrated in Figure 2-6 (Sreenivasan & Raghavan, 2002). Sreenivasan and Raghavan (2002) proved that



unlike conventional fluidized beds, which typically have two regimes of operation, three, and perhaps even four, distinct regimes of operation could be identified in the operation of the swirling fluidized bed.

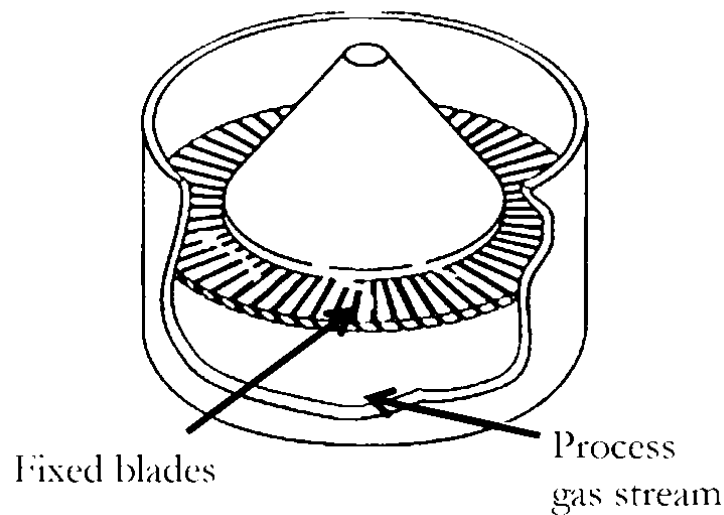


**Figure 2-5:** TORBED reactor (Torftech, sa)

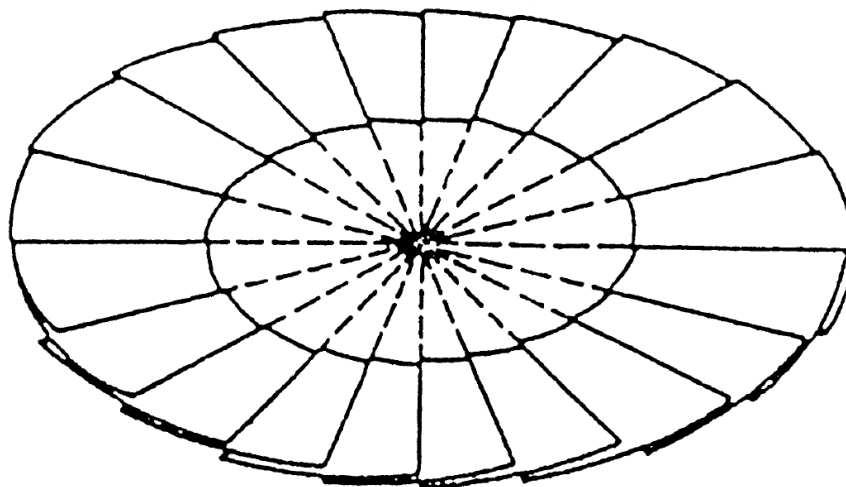


**Figure 2-6:** Fixed angled blades used as the distributor in the TORBED reactor (Sreenivasan & Raghavan, 2002)

## 2.5 Fluidized Bed Modelling

Historically, two main approaches to fluidized bed modelling have been proposed, namely pseudo-homogeneous models and two-phase models (Ho, 2003: 258). In

pseudo-homogeneous models, the existence of more than one phase is not considered. Pseudo-homogeneous models of fluidized bed reactors assume that the reactor can be modelled similarly to ideal flow models, dispersion models, residence time distribution (RTD) models or contact time distribution (CTD) models (Ho, 2003: 258).

Conversely, two-phase models assume that the fluidized bed reactor consists of at least two distinct and separate phases. Two-phase models employ a separate governing equation for each phase, which takes into account the mass interchange between the two phases (Ho, 2003: 258). Unfortunately, modelling fluidized beds using either the pseudo-homogeneous approach or the two-phase approach remains problematic – models that work for certain reactors may not work for others (Ho, 2003: 271).

In recent years, due to the advancement of computational power, computational fluid dynamics (CFD) modelling of fluidized beds has gained popularity amongst researchers. CFD modelling offers several unique advantages over empirical and phenomenological modelling, including the ability to study the fluidized bed up to and beyond expected operational limits, as well as having access to the large level of detail generated by the results (Versteeg & Malalasekera, 2007: 31). Two main approaches can be used to model fluidized beds – a Eulerian framework or Lagrangian particle tracking (Pugsley, McKeen & das Sharma, 2005). The Eulerian method is used to simulate the flow of two distinct, continuous and fully interpenetrating phases. In contrast, the Lagrangian method models the system by simulating an equation of motion of each individual particle in the system (Pugsley *et al.*, 2005). For large and complex systems, the Eulerian framework is usually more convenient to use, particularly when gases are involved. The focus is then on simulating the physical state at fixed points in space and not following the state of individual material particles.

## 2.6 References

Al-Dahhan, MH, Dudukovic, MP, Bhusarapu, S, O'hern, T, Trujillo, S and Prairie, MR (2005) “Flow Mapping in a Gas-Solid Riser via Computer Automated Radioactive Particle Tracking (CARPT)”,

<http://www.osti.gov/energycitations/servlets/purl/881590-Kfq80v/>.

Al-Hasan, M and Al-Qodah, Z (2007) “Characteristics of gas-solid flow in vertical tube”, paper presented at the *9<sup>th</sup> International Symposium on Fluid Control Measurement and Visualization*, FLUCOME 2007, 1, 264-271.

Bader, R, Findlay, J and Knowlton, TM (1988) “Gas/Solid Flow Patterns in a 30.5-cm-Diameter Circulating Fluidized Bed”, paper presented at *Circulating Fluidized Bed Technology II, Proceedings of the Second International Conference on Circulating Fluidized Beds*, 14 – 18 March 1988, Compiègne, France.

Bhusarapu, S, Al-Dahhan, MH and Dudukovic, MP (2006) “Solids flow mapping in a gas-solid riser: Mean holdup and velocity fields”, *Powder Technology*, 163(1-2), 98 – 123.

Collin, A, Wirth, KE and Ströder, M (2008) “Experimental characterization of the flow pattern in an annular fluidized bed”, *The Canadian Journal of Chemical Engineering*, 86(3), 536 – 542.

Collin, A, Wirth, KE and Ströder, M (2009) “Characterization of an annular fluidized bed”, *Powder Technology*, 190(1-2), 31 – 35.

Demori, M, Ferrari, V, Strazza, D and Poesio, P (2010) “A capacitive sensor system for the analysis of two-phase flows of oil and conductive water”, *Sensors and Actuators: A: Physical*, 163(1), 172 – 179.

Du, B, Warsito, W, Fan, LS (2005) “ECT Studies of Gas-Solid Fluidized Beds of Different Diameters”, *Industrial & Engineering Chemistry Research*, 44(14), 5020 – 5030.

Fischer, C, Peglow, M and Tsotsas, E (2011) “Restoration of particle size distributions from fibre-optic in-line measurements in fluidized bed processes”, *Chemical Engineering Science*, 66(12), 2842 – 2852.

Fraguío, MS, Cassanello, MC, Degaleesan, S and Dudukovic, MP (2009) “Flow regime diagnosis in bubble columns via pressure fluctuations and computer-assisted radioactive particle tracking measurements”, *Industrial and Engineering Chemistry Research*, 48(3), 1072 – 1080.

Franka, NP and Heindel, TJ (2009) “Local time-averaged gas holdup in a fluidized bed with side air injection using X-ray computed tomography”, *Powder Technology*, 193(1), 69 – 78.

Fu, Y, Wang, T, Chen, JC, Gu, CG and Xu, F (2011) “Experimental investigation of jet influence on gas-solid the two-phase crossflow in a confined domain”, *Shiyan Lixue/Journal of Experiments in Fluid Mechanics*, 25(1), 48 – 53, 64.

Geldart, D (1973) “Types of fluidization”, *Powder Technology*, 7, 285 – 292.

Guo, Q and Werther, J (2008) “Influence of a gas maldistribution of distributor design on the hydrodynamics of a CFB riser”, *Chemical Engineering and Processing: Process Intensification*, 47(2), 237 – 244.

He, Y, Deen, NG, van Sint Annaland, M and Kuipers, JAM (2009) “Gas-solid turbulent flow in a circulating fluidized bed riser: experimental and numerical study of monodisperse particle systems”, *Industrial & Engineering Chemistry Research*, 48(17), 8091 – 8097.

Hernández-Jiménez, F, Sánchez-Delgado, S, Gómez-García, A and Acosta-Iborra, A (2011) “Comparison between two-fluid model simulations and particle image analysis & velocimetry (PIV) results for a two-dimensional gas-solid fluidized bed”, *Chemical Engineering Science*, 66(17), 3753 – 3772.

Ho, TC (2003) *Modeling*, In Yang, W (ed) *Handbook of Fluidization and Fluid-Particle Systems*, Marcel Dekker, Inc, United States of America.

Ibsen, CH, Solberg, T and Hjertager, BH (2001) “Evaluation of a three-dimensional numerical method of a scaled circulating fluidized bed”, *Industrial and Engineering Chemistry Research*, 40(23), 5081 – 5086.

Ibsen, CH, Solberg, T, Hjertager, BH and Johnsson, F (2002) “Laser Doppler anemometry measurements in a circulating fluidized bed of metal particles”, *Experimental Thermal and Fluid Science*, 26(6-7), 851 – 859.

Jazayeri, B (1995) “Successful scale up catalytic gas-fluidized beds”, *Chem Eng Prog*, 91(4), 26 – 31.

Jiang, P, Wei, F and Fan, L (2003) *General Approaches to Reactor Design*, In Yang, W (ed) *Handbook of Fluidization and Fluid-Particle Systems*, Marcel Dekker, Inc, United States of America.

Kashyap, M and Gidaspow, D (2011) “Measurements of dispersion coefficients for FCC particles in a free board” *Industrial & Engineering Chemistry Research*, 50(12), 7549 – 7565.

Khanna, P, Pugsley, T, Tanfara, H and Dumont, H (2008) “Radioactive particle tracking in a lab-scale conical fluidized bed dryer containing pharmaceutical granule”, *The Canadian Journal of Chemical Engineering*, 86(3), 563 – 570.

Krishna, R (1994) “A systems approach to multiphase reactor selection”, *Advances Chem Eng*, 19, 201 – 249.

Kuan, B, Yang, W and Schwarz, MP (2007) “Dilute gas-solid two-phase flows in a curved 90° duct bend: CFD simulation with experimental validation” *Chemical Engineering Science*, 62(7), 2068 – 2088.

Kumar, SB, Moslemian, D and Dudukovic, MP (1995) “A [gamma]-ray tomographic scanner for imaging voidage distribution in two-phase flow systems”, *Flow Measurement and Instrumentation*, 6(1), 61 – 73.

Kunii, D and Levenspiel, O (1991) *Fluidization Engineering*, 2nd Edition, Butterworth-Heinemann Series in Chemical Engineering, Stoneham, MA.

Larachi, F, Al-Dahhan, MH, Dudukovic, MP and Roy, S (2008) “Optimal design of radioactive particle tracking experiments for flow mapping in opaque

multiphase reactors”, *Applied Radiation and Isotopes Including Data Instrumentation and Methods for Use in Agricultural Industry and Medicine*, 56(3), 485 – 503.

Laverman, JA, Roghair, I, van Sint Annaland, M and Kuipers, H (2008) “Investigation into the hydrodynamics of gas-solid fluidized beds using particle image velocimetry coupled with digital image analysis”, *The Canadian Journal of Chemical Engineering*, 86(3), 523 – 535.

Link, JM, Godlieb, W, Tripp, P, Deen, NG, Heinrich, S, Kuipers, JAM, Schönherr, M and Peglow, M (2009) “Comparison of fibre optical measurements and discrete element simulations for the study of granulation in a spout fluidized bed”, *Powder Technology*, 189(2), 202 – 217.

Lu, Y, Glass, DH and Easson, WJ (2009) “An investigation of particle behaviour in gas-solid horizontal pipe flow by an extended LDA technique”, *Fuel*, 88(12), 2520 – 2531.

Mathiesen, V, Solberg, T, Arastoopour, H and Hjertager, BH (1999) “Experimental and computational study of multiphase gas/particle flow in a CFB riser”, *AIChE Journal*, 45(12), 2503 – 2518.

Meggitt, BT (2010) *Fibre Optics in Sensor Instrumentation*, In *Instrumentation Reference Book*, Fourth Edition, 191 – 216, Butterworth-Heinemann, Boston.

Newton, D, Fiorentino, M and Smith, GB (2001) “The application of X-ray imaging to the developments of fluidized bed processes”, *Powder Technology*, 120(1-2), 70 – 75.

Paudel, BE (2011) *Experimental study on fluidization of biomass, inert particles and biomass/sand mixtures*, MSc Thesis, Department of Mechanical and Energy Engineering, University of North Texas.

Pell, W, Dunson, JB and Knowlton, TM (2007) *Gas-solid operations and equipment*, In Green, DW and Perry, RH (eds) *Perry's Chemical Engineers' Handbook*, 8th Edition, McGraw-Hill.

Petritsch, G, Reinecke, N and Mewes, D (2000) *Visualization techniques in process engineering*, In *Ullmann's Encyclopaedia of Industrial Chemistry*, Wiley-VCH Verlag GmbH & Co KGaA.

Pugsley, T, McKeen, T and das Sharma, S (2005) "Application of CFD to simulate the hydrodynamics of fluidized beds containing fine powders", a paper presented at the *Industrial Fluidization South Africa Conference*, 16 – 17 November, 2005, Johannesburg, South Africa.

Rhodes, M (2008) *Introduction to Particle Technology*, 2<sup>nd</sup> Edition, John Wiley & Sons Ltd, England.

Richardson, JF, Harker, JH and Backhurst, JR (2002) *Coulson and Richardson's Chemical Engineering, Volume 2: Particle Technology and Separation Processes*, 5th Edition, Butterworth-Heinemann, Oxford.

Sathe, MJ, Thaker, IH, Stand, TE and Joshi, JB (2010) "Advanced PIV/LIF and shadowgraphy system to visualize flow structure in two-phase bubbly flows", *Chemical Engineering Science*, 65(8), 2431 – 2442.



Silva, GG, Jiménez, NP and Salazar, OF (2012) *Fluid dynamics of gas-solid fluidized beds*, In Oh, HW (ed) *Advanced Fluid Dynamics*, InTech.

Sreenivasan, B and Raghavan, VR (2002) “Hydrodynamics of a swirling fluidized bed”, *Chemical Engineering and Processing*, 41, 99 – 106.

Tan, HT, Dong, GG, Wei, YD and Shi, MX (2007) “Application of  $\gamma$ -ray attenuation technology in measurement of solid concentration of gas-solid two-phase flow in a FCC riser”, *Guocheng Gongcheng Xuebao/ Chinese Journal of Process Engineering*, 7(5), 895 – 899.

Tapp, HS, Peyton, AJ, Kemsley, EK and Wilson (2003) “Chemical engineering applications of electrical process tomography”, *Sensors and Actuators, B: Chemical*, 92(1-2), 17 – 24.

Thatte, AR, Ghadge, RS, Patwardhan, AW, Joshi, JB and Singh, G (2004) “Local gas holdup measurement in sparged and aerated tanks by  $\gamma$ -ray attenuation technique”, *Industrial & Engineering Chemistry Research*, 43(17), 5389 – 5399.

Torftech (sa) “TORBED Compact Bed Reactor (‘CBR’)”,  
[http://www.torftech.com/technologies/compact\\_bed\\_reactor.html](http://www.torftech.com/technologies/compact_bed_reactor.html) [Accessed 8 October 2014].

Vaishali, S, Roy, S, Bhusarapu, S, Al-Dahhan, MH and Dudukovic, MP (2007) “Numerical simulation of gas-solid dynamics in a circulating fluidized-bed riser with Geldart group B particles”, *Industrial and Engineering Chemistry Research*, 46(25), 8620 – 8628.

Van Buijtenen, MS, van Dijk, WJ, Deen, NG, Kuipers, JAM, Leadbeater, T and Parker, DJ (2011) “Numerical and experimental study on multiple-spout fluidized beds”, *Chemical Engineering Science*, 66(11), 2368 – 2376.

Veluswamy, GK, Upadhyay, RK, Utikar, RP, Evans, GM, Tade, MO, Glenny, ME, Roy, S and Pareek, VK (2011) “Hydrodynamics of a fluid catalytic cracking stripper using  $\gamma$ -ray densitometry” *Industrial & Engineering Chemistry Research*, 50(10), 5933 – 5941.

Versteeg, HK and Malalasekera, W (2007) *An introduction to computational fluid dynamics: the finite volume method*, 2nd Edition, Pearson Education Limited, Essex.

Vogt, C, Schreiber, R, Brunner, G and Werther, J (2005) “Fluid dynamics of the supercritical fluidized bed”, *Powder Technology*, 158(1-3), 102 – 114.

Wang, HG, Yang, WQ, Senior, P, Raghavan, RS and Duncan, SR (2008) “Investigation of batch fluidized-bed drying by mathematical modelling, CFD simulation and ECT measurement”, *AIChE Journal*, 54(2), 427 – 444.

Wang, RC and Han, YC (1999) “Momentum dissipation of jet dispersion in a gas-solid fluidized bed”, *Journal of the Chinese Institute of Chemical Engineers*, 30(3), 263 – 271.

Wang, Z, Sun, S, Chen, H, Deng, Q, Zhao, G and Wu, S (2009) “Experimental investigation on flow asymmetry in solid entrance region of a square circulating fluidized bed”, *Particuology*, 7(6), 483 – 490.

Werther, J and Hartge, E (2003) *Elutriation and entrainment*, In Yang, W (ed) *Handbook of fluidization and fluid-particle systems*, Marcel Dekker, Inc, United States of America.

Werther, J and Reppenhagen, J (2003) *Attrition*, In Yang, W (ed) *Handbook of fluidization and fluid-particle systems*, Marcel Dekker, Inc, United States of America.

Werther, J, Hage, B and Rudnick, C (1996) “A comparison of laser Doppler and single-fibre reflection probes for the measurement of the velocity of solids in a gas-solid circulating fluidized bed”, *Chemical Engineering and Processing: Process Intensification*, 35(5), 381 – 391.

Wiesendorf, V (2000) *The capacitance probe: a tool for flow investigations in gas-solids fluidization systems*, Shaker Verlag GmbH, Germany.

Wu, C, Cheng, Y, Liu, M and Jin, Y (2008) “Measurement of axisymmetric two-phase flows by an improved X-ray-computed tomography technique”, *Industrial and Engineering Chemistry Research*, 47(6), 2063 – 2074.

Yang, W (2003) *Other Nonconventional Fluidized Beds*, In Yang, W (ed) *Handbook of fluidization and fluid-particle systems*, Marcel Dekker, Inc, United States of America.

Ye, S, Qi, X and Zhu, J (2009) “Direct measurements of instantaneous solid flux in a CFB riser using a novel multifunctional optical fiber probe”, *Chemical Engineering & Technology*, 32(4), 580 – 589.

Zhou, H, Mo, G, Zhao, J, Li, J and Cen, K (2010) “Experimental investigations on the performance of a coal pipe splitter for a 1 000 MW utility boiler: influence of the vertical pipe length” *Energy & Fuels*, 24(9), 4893 – 4903.

Zhu, H, Zhu, J, Li, G and Lu, F (2008) “Detailed measurements of flow structure inside a dense gas-solids fluidized bed”, *Powder Technology*, 180(3), 339 – 349.

---

# CHAPTER 3: MATERIALS & METHODS

---

Before starting experimental work, the hydrodynamic behaviour of any fluidized bed can be predicted, provided that several characteristics of the bed of particles, and those of the individual particles themselves, are known. These characteristics include the mean particle size, the individual particle density as well as the particle sphericity.

River sand was selected as the primary material tested in the annular fluidized bed as it would also be the bed material used in the pyrolysis chamber of the new fluidized bed fast pyrolyser. In order to compare the behaviour of the annular fluidized bed using materials of varying particle sizes and bulk densities, additional materials, namely ilmenite, an ilmenite-sand mixture, mustard seeds and poppy seeds, were also tested.

The particle size distribution of the various materials tested was determined using laser diffraction in a Malvern Mastersizer 3000, and a scanning electron microscope (Phenom ProX desktop SEM) was used to study the individual particles in more detail. A summary of the findings can be found at the end of this Chapter (Table 3-1). A brief discussion on the flow of air and how the pressure drop measurements were obtained is also described in this Chapter.

## 3.1 River Sand

The river sand obtained for the experiments was initially sieved through a 2 mm mesh screen in order to remove large, unwanted particles. Thereafter, the particle size distribution (Figure 3-1), as well as the particle density, was determined. Based on Figure 3-1, it is evident that the sieved river sand sample had a large particle size distribution, with a volume average particle size of 528  $\mu\text{m}$ . The bulk density of the

sieved river sand was determined to be  $1\,350\text{ kg/m}^3$ , and the particle density of the individual sand particles was determined to be  $2\,070\text{ kg/m}^3$ .

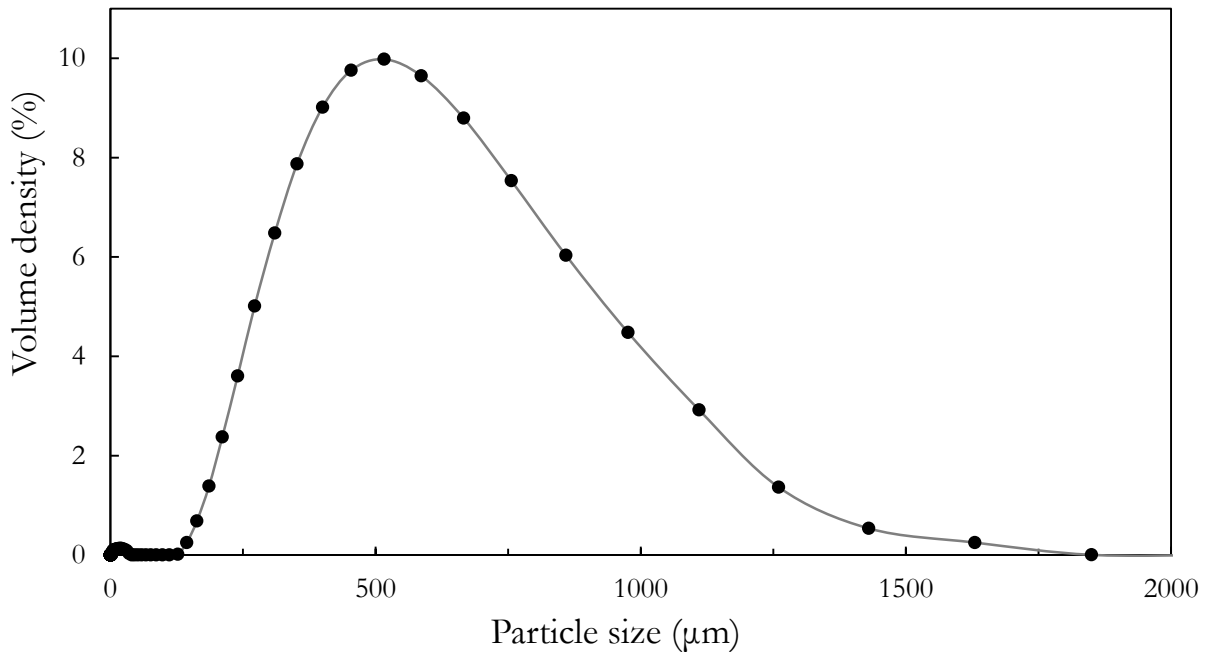


**Figure 3-1:** Particle size distribution of river sand

The SEM images of the sieved river sand revealed that the individual sand particles were angular in shape with sharp edges, as illustrated in Figure 3-2. Although some sand particles did have smooth surfaces, the majority of particles had rough surfaces.

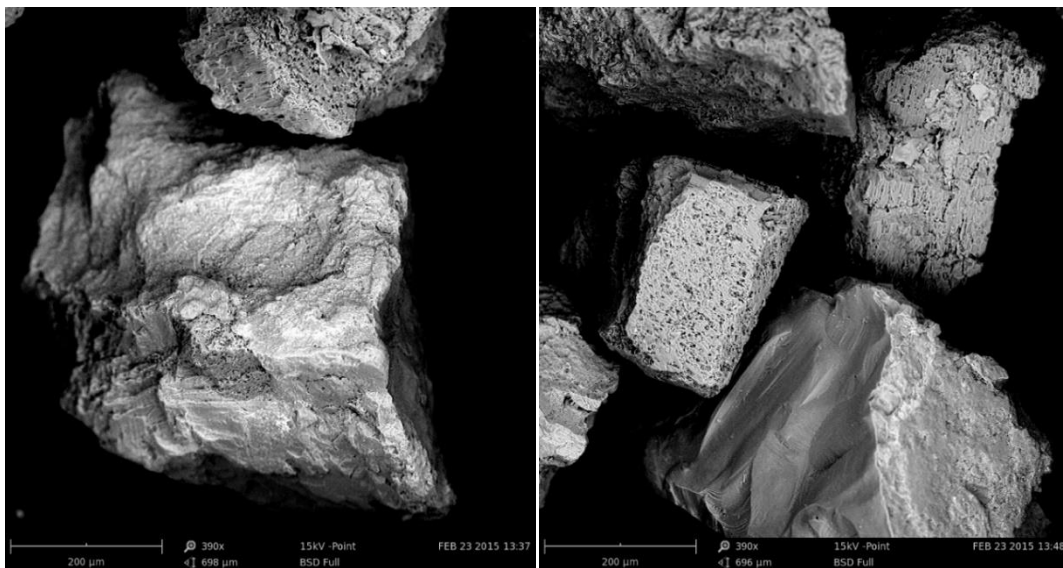


**Figure 3-2:** SEM images of river sand

### 3.2 Additional Materials

The particle size distribution of ilmenite (a weakly magnetic titanium-iron oxide material) and the ilmenite-sand mixture is illustrated in Figure 3-3. In comparison to the particle size distribution of the sieved river sand in Figure 3-1, the ilmenite and the ilmenite-sand mixture had significantly smaller particle size distributions. The volume average particle sizes of the ilmenite and the ilmenite-sand mixture were determined to be 142  $\mu\text{m}$  and 165  $\mu\text{m}$  respectively.

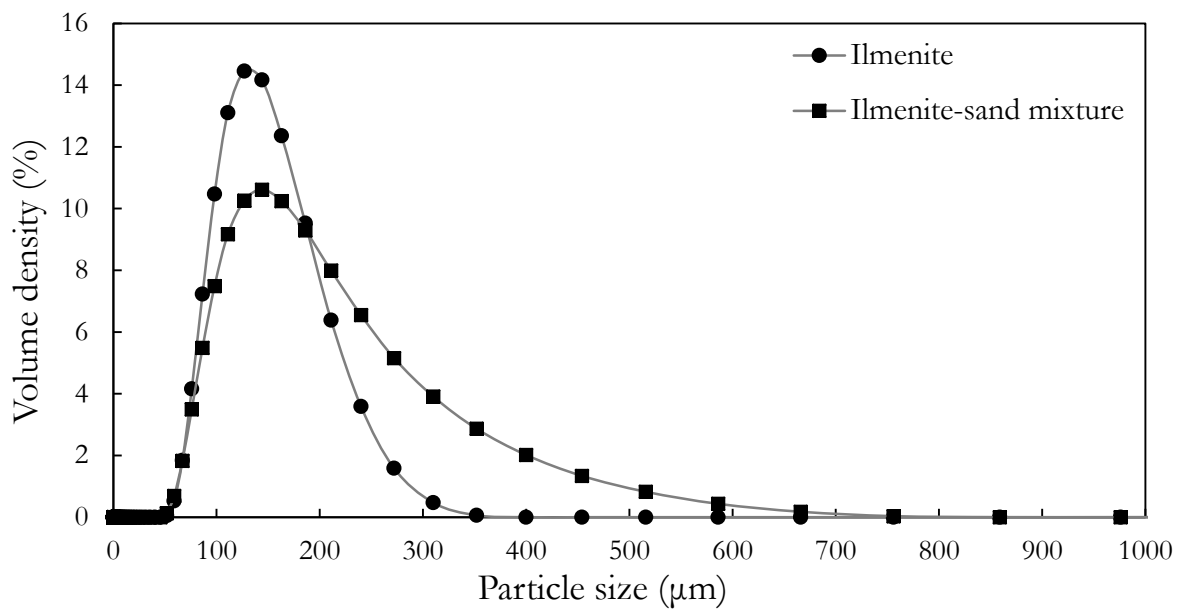


**Figure 3-3:** Particle size distribution of the ilmenite and the ilmenite-sand mixture

The bulk density of the ilmenite was determined to be 2 780  $\text{kg}/\text{m}^3$ , whereas the particle density of the individual ilmenite particles was determined to be 4 630  $\text{kg}/\text{m}^3$ . Likewise, the bulk density of the ilmenite-sand mixture was determined to be 2 230  $\text{kg}/\text{m}^3$ , whereas the particle density of the individual ilmenite and sand particles in the mixture was determined to be approximately 3 690  $\text{kg}/\text{m}^3$ . The SEM images of the ilmenite (Figure 3-4) and the ilmenite-sand mixture (Figure 3-5) revealed that the individual ilmenite particles were rounded with smooth edges and surfaces. Conversely, the sand contained in the ilmenite-sand mixture was determined to be angular with sharp edges, similar to that shown in Figure 3-2.





Figure 3-4: SEM images of ilmenite

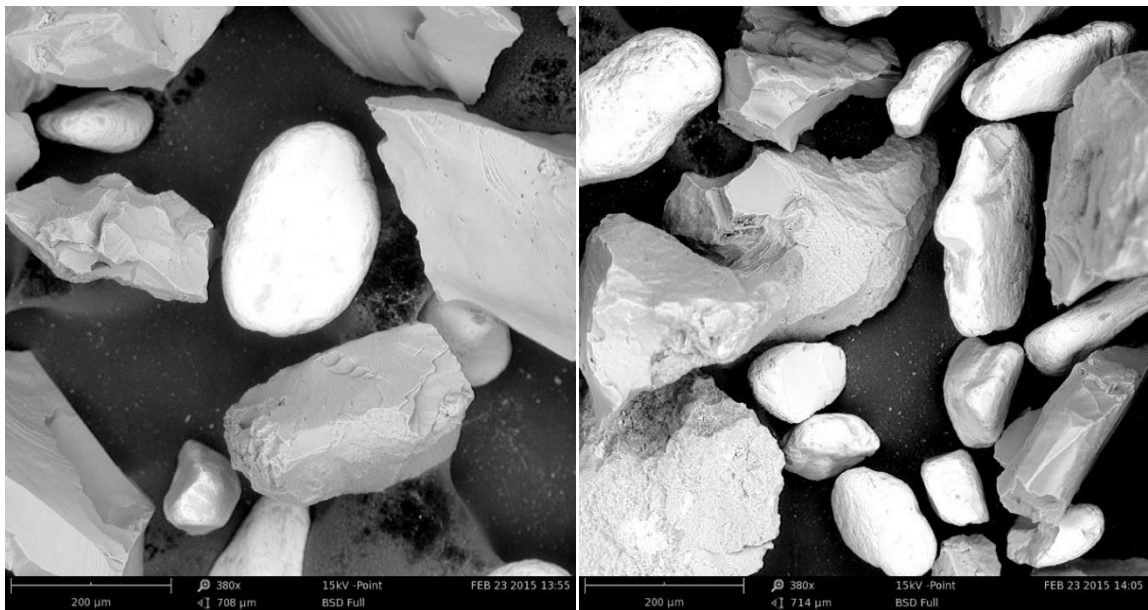
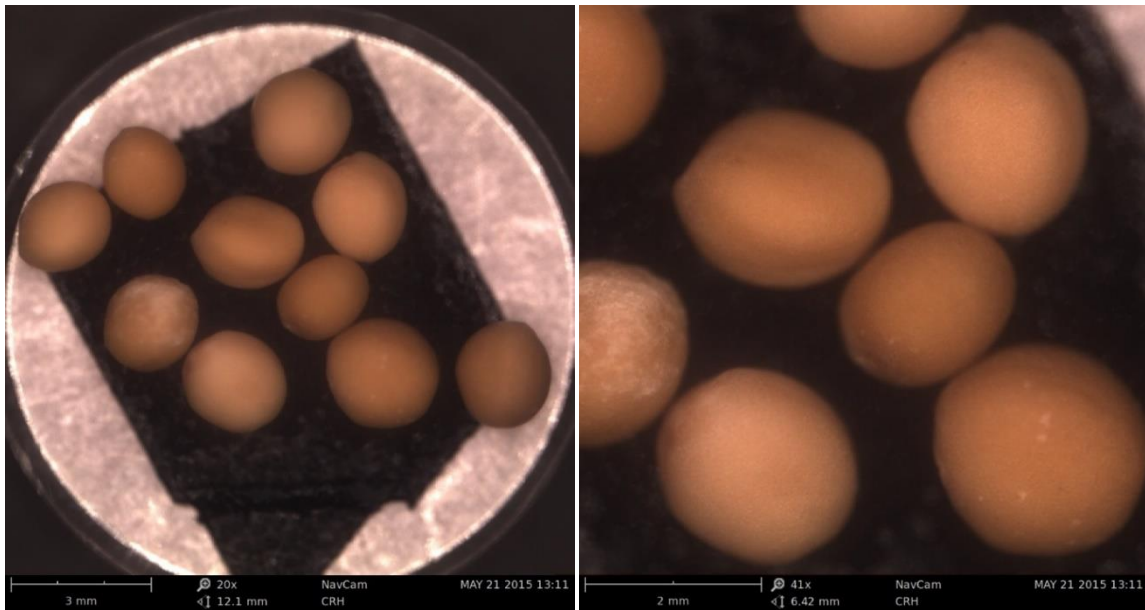


Figure 3-4: SEM images of ilmenite-sand mixture

Particle size distributions were not determined for mustard seeds or poppy seeds, since it was observed that both types of seed had uniform particle sizes. For this reason, the individual particle sizes of the mustard seeds and poppy seeds were determined by visual inspection to be 2 mm and 1 mm respectively. The bulk density of the mustard seeds was determined to be  $760 \text{ kg/m}^3$ , whereas the particle density of the individual mustard seeds was determined to be  $950 \text{ kg/m}^3$ . Likewise, the bulk



density of the poppy seeds was determined to be  $680 \text{ kg/m}^3$ , whereas the particle density of the individual poppy seeds was determined to be  $850 \text{ kg/m}^3$ . The SEM images of the mustard seeds revealed that the individual seeds were spherical with smooth edges, as illustrated in Figure 3-6. The poppy seeds were also observed to be mostly spherical with an uneven surface under the SEM (Figure 3-7).



**Figure 3-5:** SEM images of mustard seeds

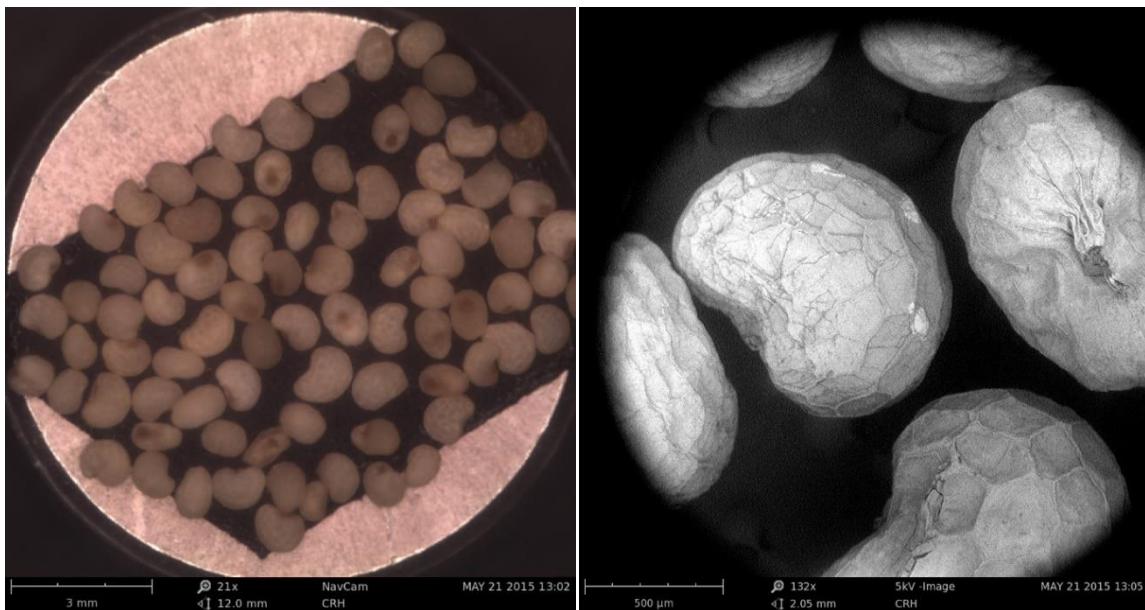


**Figure 3-6:** SEM images of poppy seeds

### 3.3 Pressure Drop Measurements

The annular fluidized bed was constructed of two Perspex tubes of equal length but of different diameters. The smaller Perspex tube was placed inside the larger Perspex tube, creating a vertically orientated annulus, and a base manufactured from mild steel secured the two tubes in place. The Perspex model setup comprised a 1.75 kW double-stage side-channel blower connected to a variable speed controller; two manometers with a bidirectional orifice plate used for determining the superficial gas velocity of the fluidizing air; and a rolled stainless steel pipe which distributed the air into 16 tapped holes (Figure 3-8). All pressure drops were measured in millimetres of water using two adjacent manometers.

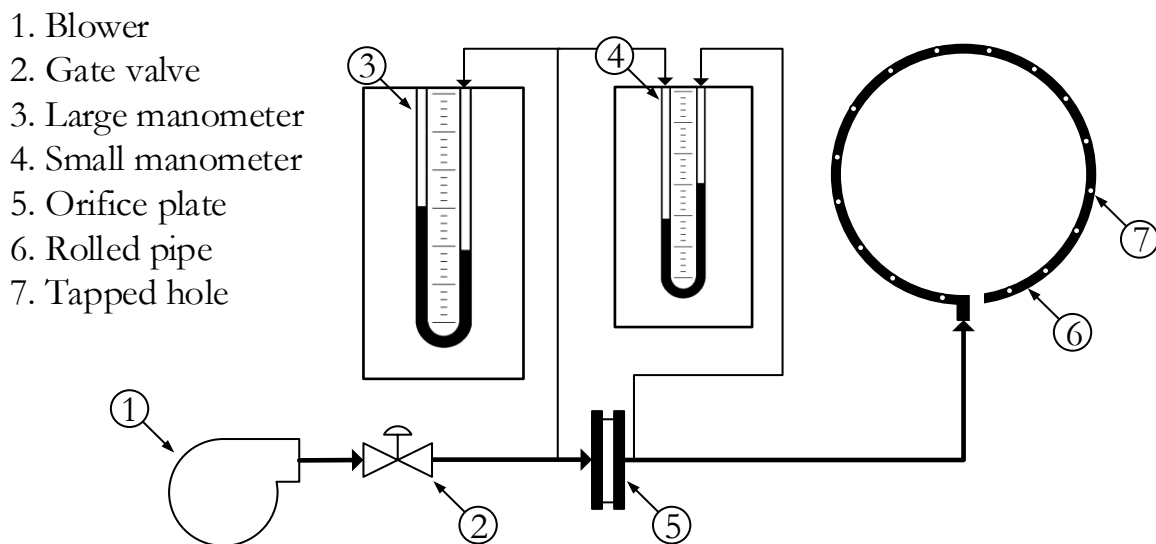


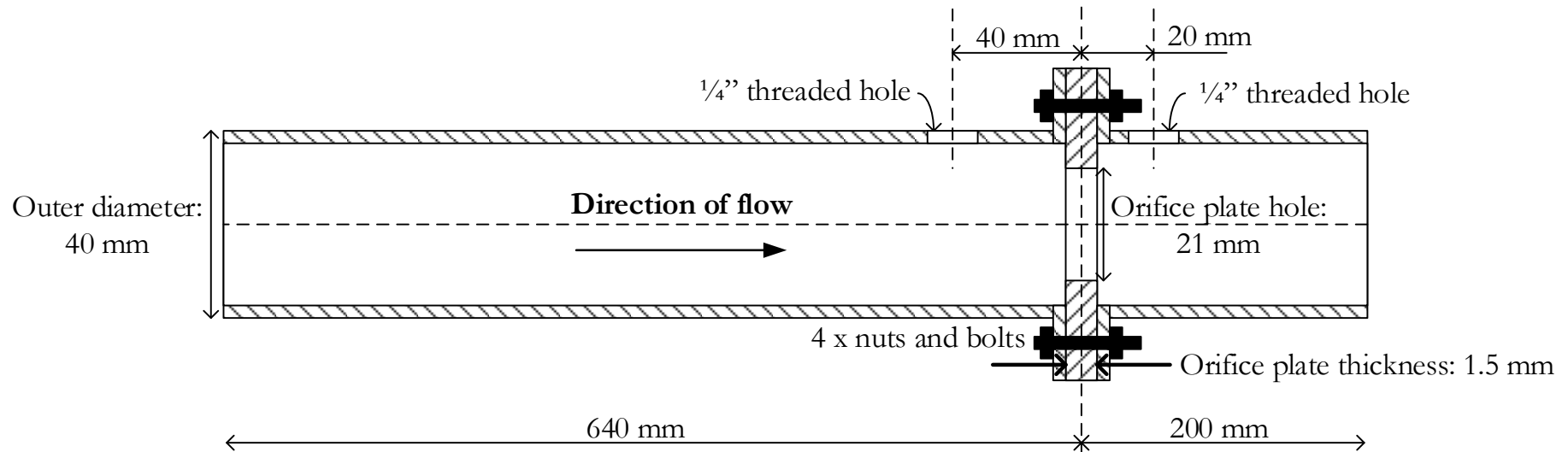
**Figure 3-7:** Schematic diagram of air flow from double-stage side-channel blower to tapped holes in rolled stainless steel pipe

The bidirectional orifice plate hole was initially designed to be 14 mm in diameter; however, during calibration, it was noticed that the pipe directing the fluidizing air heated up, and the attached manometers were too short to provide readings at high superficial gas velocities. For these reasons, the orifice plate hole was slightly widened to 21 mm, as illustrated in Figure 3-9.

**Table 3-1:** Summary of characteristics of materials used in experiments

| Material/Property                          | Ilmenite | Ilmenite-sand mixture | River sand | Mustard seeds | Poppy seeds |
|--|----------|-----------------------|------------|---------------|-------------|
| <b>D<sub>v50</sub> (mm)</b>                | 0.142    | 0.165                 | 0.528      | 2*            | 1*          |
| <b>D<sub>v10</sub> (mm)</b>                | 0.092    | 0.094                 | 0.269      | -             | -           |
| <b>D<sub>v90</sub> (mm)</b>                | 0.220    | 0.326                 | 0.972      | -             | -           |
| <b>Bulk density (kg/m<sup>3</sup>)</b>     | 2 780    | 2 230                 | 1 350      | 760           | 680         |
| <b>Particle density (kg/m<sup>3</sup>)</b> | 4 530    | 3 690                 | 2 070      | 950           | 850         |
| <b>Geldart Group classification</b>        | B        | B                     | B          | D             | B           |

\*Determined by visual inspection



# CHAPTER 4: TANGENTIAL INJECTORS

By orientating multiple gas injectors tangentially to the outer walls of an annulus, it was hypothesized that the centrifugal forces and the momentum transfer between the moving gas to the bed material would be sufficient to induce a rotating fluid bed. Annular fluidized beds with induced rotating fluid bed behaviour would ensure complete mixing, and offer the additional advantage that the feed inlet to the fluidized bed can be positioned at a single location.

## 4.1 Design Concept

It was hypothesized that the direction of the induced rotating fluid bed (clockwise or anti-clockwise) would depend on the orientation of the gas injectors as illustrated in Figure 4-1. The momentum transfer between the moving gas and the bed of particles would depend on the number of gas injectors placed around the annulus, the angle of the gas injectors, as well as the size of the gas injectors. The linear velocity of the gas entering the annulus through the gas injectors would be determined by the diameter of the gas injectors.

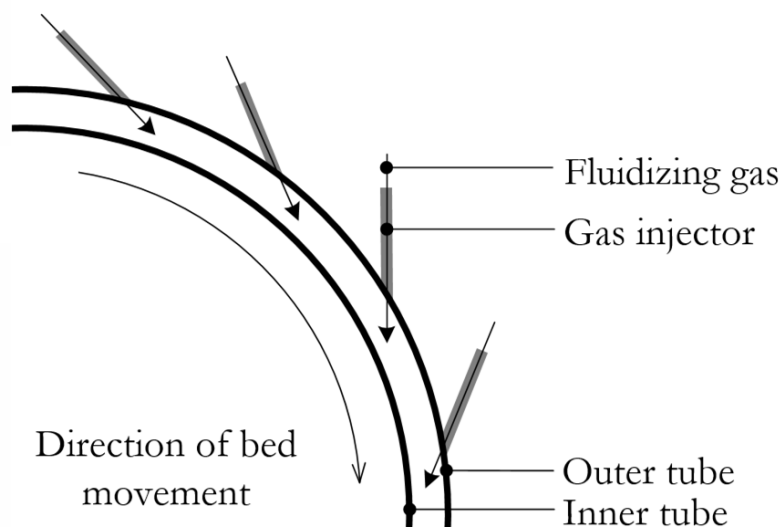


**Figure 4-1:** Clockwise rotation of the fluid bed in an annular space

## 4.2 Construction

The fluidizing air flowing from the tapped holes in the rolled pipe (refer to Figure 3-9) was directed to 16 Perspex air injector housings, as illustrated in Figure 4-2. The air injector housings were attached to the exterior surface of the outer Perspex tube, 30 mm above the base of the model. Copper pipes were screwed into the air injector housings, which guided the air into the annulus tangentially to the inner wall of the outer Perspex tube.

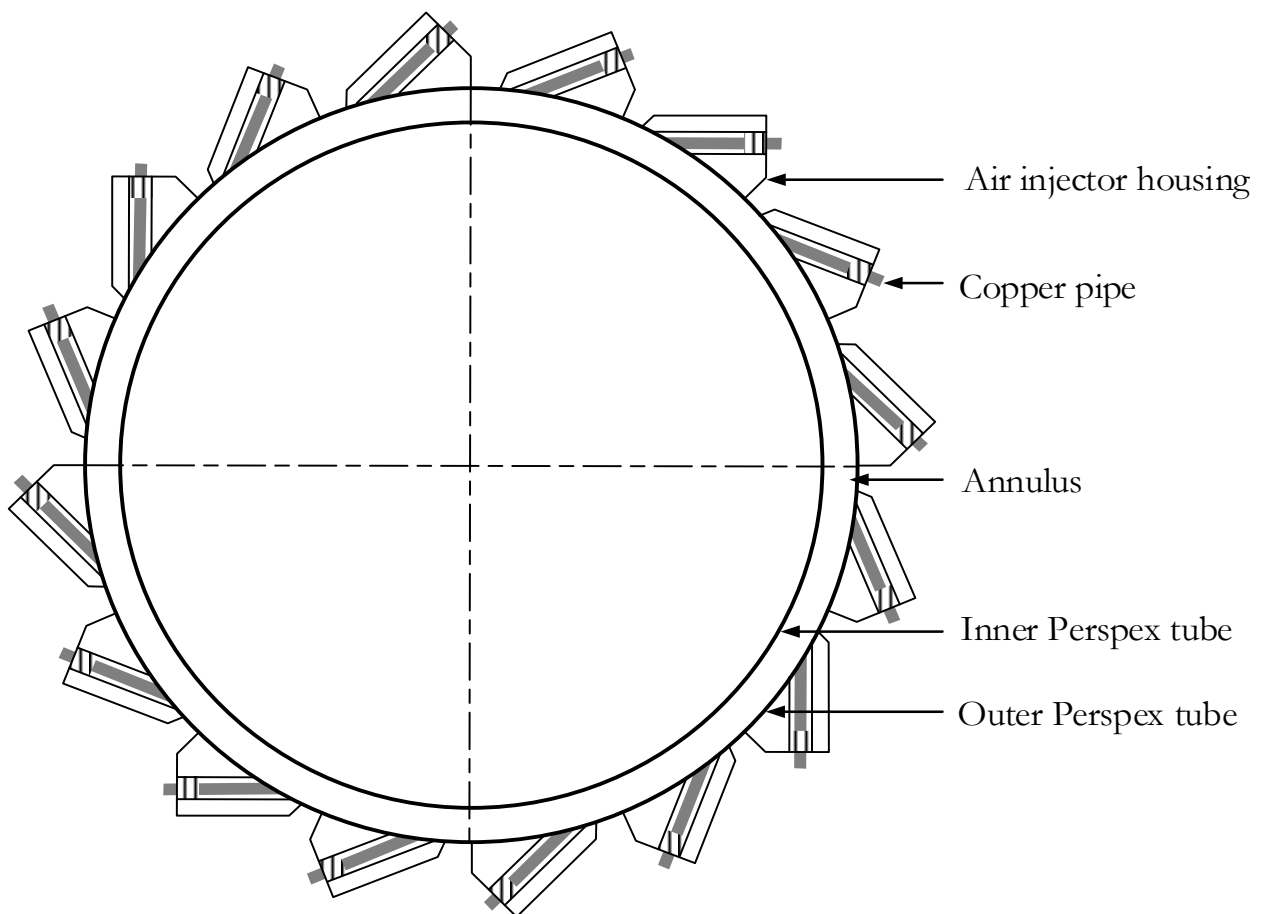


**Figure 4-2:** Detailed diagram of the air injector housings with copper pipes

The dimensions and specifications of the individual parts used in the Perspex model setup are summarised in Table 4-1. Figure 4-3 shows a photograph of the assembled Perspex model.

**Table 4-1:** Dimensions and specifications of parts used in the Perspex model setup

| Specification                     | Value                | Units |
|-----------------------------------|----------------------|-------|
| Outer Perspex tube inner diameter | 0.44                 | m     |
| Inner Perspex tube outer diameter | 0.4                  | m     |
| Perspex tube wall thickness       | $5 \times 10^{-3}$   | m     |
| Perspex tube height               | 1                    | m     |
| Number of air injector housings   | 16                   | -     |
| Copper pipe inner diameter        | $6.5 \times 10^{-3}$ | m     |

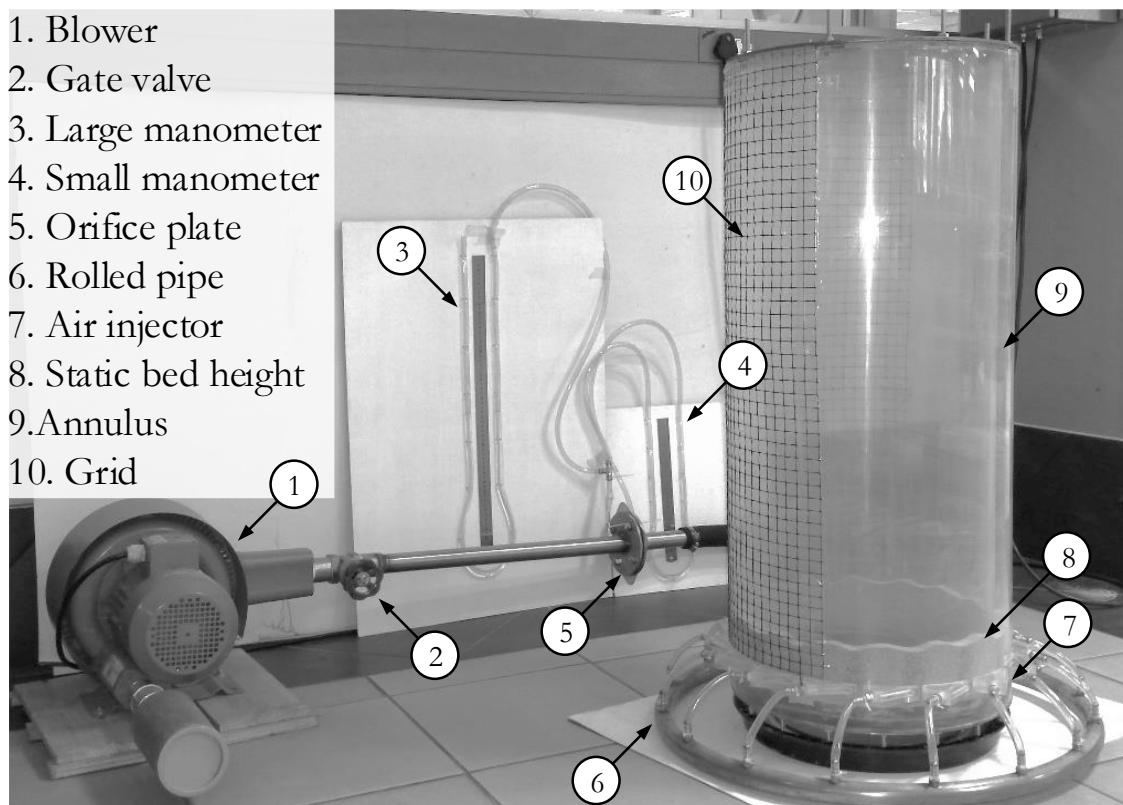


**Figure 4-3:** Photograph of the assembled Perspex model

### 4.3 Initial Experiments

In the initial experiments of the assembled Perspex model, the superficial gas velocity was gradually increased using the variable speed controller with no bed



material in the annulus. This test was performed in order to ensure that the double-stage side-channel blower was operating properly, all 16 gas injectors were delivering the fluidizing air, and that no air leaks could be detected outside of the annulus. Controlled amounts of river sand were then loaded into the annulus and the same test was repeated. Some static charge was observed, resulting in several river sand particles sticking to the inner walls of the annulus. However, this phenomenon was determined to be insignificant as only a small proportion of particles were affected.

Charging less than 2.5 kg of river sand proved to be problematic as the uneven pressure drop in the rolled pipe caused the complete removal of the river sand at several air injectors. The removed river sand was initially suspended and swirled around the annulus in a manner similar to pneumatic conveying. However, accumulation of river sand at other air injectors inevitably occurred, and the suspended river sand eventually settled on the build-up, as illustrated in Figure 4-4.

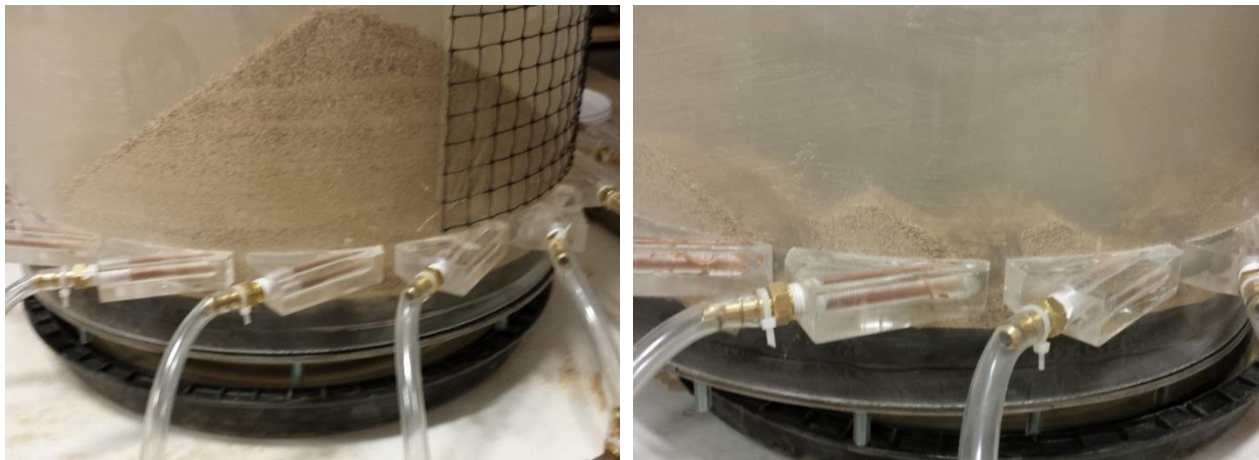


**Figure 4-4:** (*Left*) Bed material removed at several air injectors (2.0 kg river sand); (*right*) accumulation of bed material at other air injectors (2.0 kg river sand)

The observations illustrated in Figure 4-4 can be further explained with the aid of Figure 4-5, which depicts the pressure along the length of the rolled pipe as a function of the volumetric air flow rate. At the start of the rolled pipe, the air enters at maximum volume and pressure. As the air gets distributed to the tapped holes

and into the air injectors placed around the annulus, the pressure and volumetric flow rate of the air decreases to a minimum at the end of the rolled pipe. This implies that the air directed to the first few air injectors at the start of the rolled pipe will be at higher pressure compared to the air directed to the last remaining air injectors at the end of the rolled pipe.

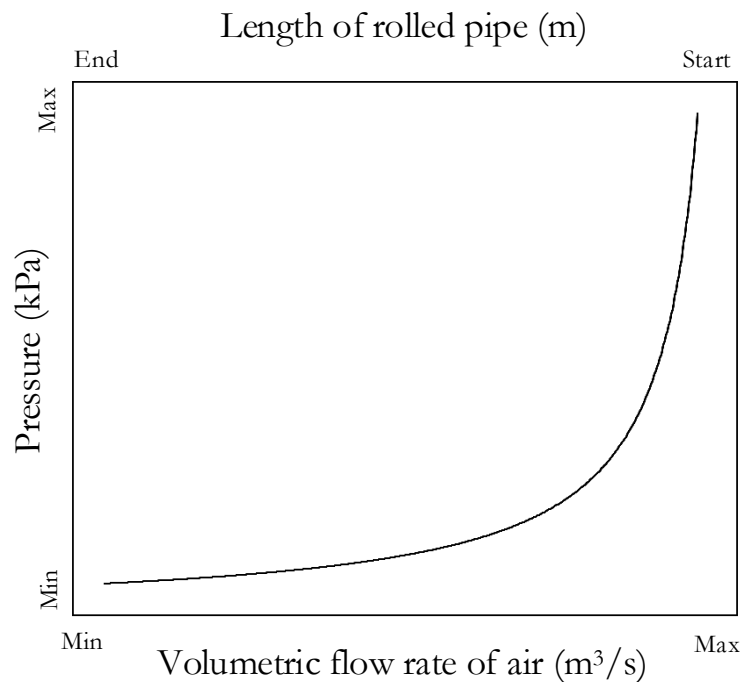


**Figure 4-5:** Pressure along the length of the rolled pipe as a function of the volumetric flow rate of the air

In the event that the bed material only just covers the air injectors as in Figure 4-4, the increased pressure at the first few air injectors will be sufficient to completely displace the surrounding bed material away from the air injector. This displacement of bed material will inevitably result in the accumulation of bed material at other air injectors, causing them to become blocked. Once one air injector is blocked, the volume of the air in the rolled pipe is then redistributed amongst the remaining air injectors, exacerbating the uneven distribution of air in the fluidized bed. It was therefore concluded that, before the experiments were started, it was necessary to ensure that each air injector was equally covered in bed material, and that sufficient bed material for fluidization was above the air injectors.



## 4.4 Results and Discussion

Four experiments were conducted: the river sand charged into the annulus was increased from 2.5 kg to 4.0 kg in 0.5 kg increments, using the assembled Perspex model with multiple tangential air injectors. For each sand loading charged into the annulus, the superficial gas velocity was gradually increased and the bed expansion measured optically, as illustrated in Figure 4-6.

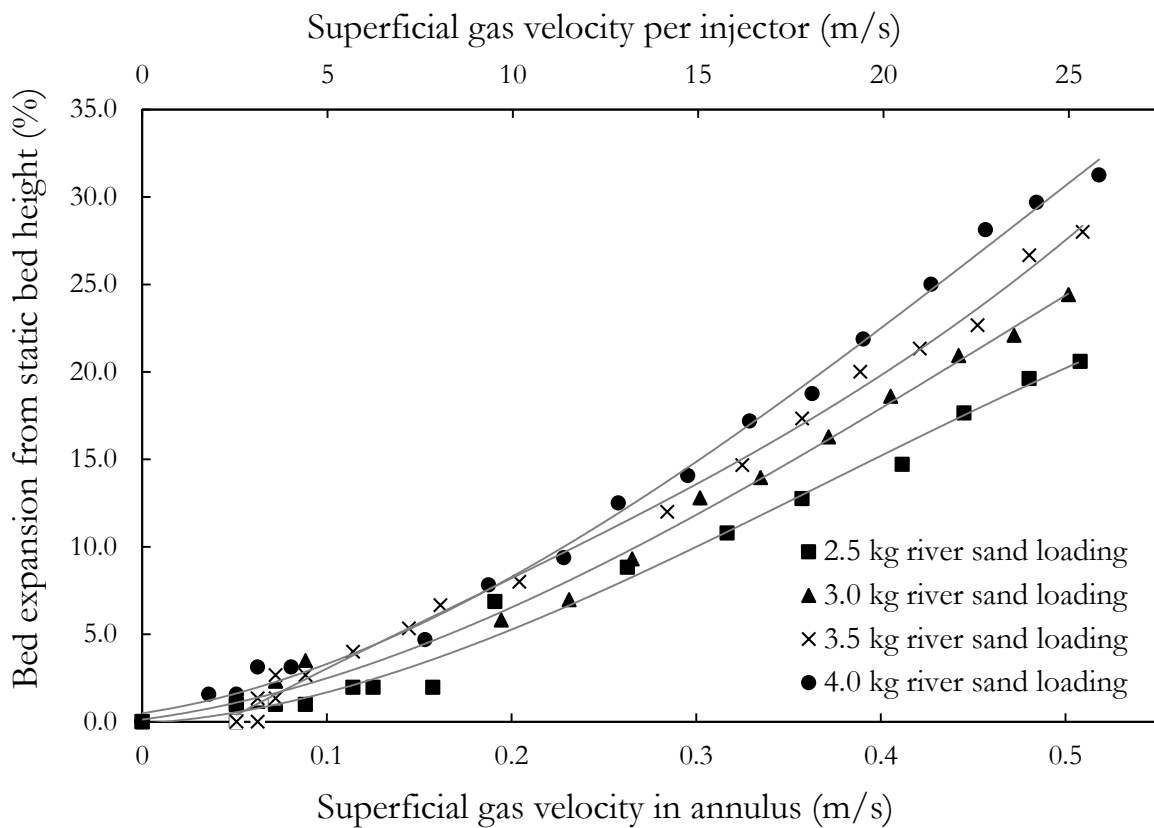


**Figure 4-6:** Comparison of bed expansion of river sand from static bed height as a function of superficial gas velocity

The bed height and superficial gas velocity at minimum fluidization for each sand loading are summarized in Table 4-2. At the start of each experiment, entrainment of fine solids contained in the sieved river sand was noticed, which reduced the particle size distribution of the river sand in the annulus. The majority of these fine solids were removed from the annular fluidized bed at low superficial gas velocities, below 0.1 m/s in the annulus.

**Table 4-2:** Summary of river sand experimental results

|   | <b>River sand loading</b> |        |        |        |
|---|---------------------------|--------|--------|--------|
|   | 2.5 kg                    | 3.0 kg | 3.5 kg | 4.0 kg |
| <b>Static bed height (mm)</b>                           | 65                        | 75     | 86     | 102    |
| <b>Minimum fluidization velocity in annulus (m/s)</b>   | 0.15                      | 0.19   | 0.23   | 0.26   |
| <b>Bed height at minimum fluidization velocity (mm)</b> | 67                        | 80     | 92     | 112    |

Based on the experimental results depicted in Figure 4-6 and summarized in Table 4-2, it is evident that with increasing superficial gas velocity, the rate of bed expansion is proportional to the river sand loading. Furthermore, the minimum fluidization velocity was also found to be proportional to the river sand loading. These results can both be explained by the fact that the fluidizing air requires increasingly more energy to impart momentum to the river sand particles as the mass of the bed increases.

The hydrodynamic behaviour of the annular fluidized bed merits further discussion. Initially, it was thought that orientating the air injectors tangentially to the inner wall of the outer Perspex tube would induce a rotating fluid bed. Unfortunately, for all four river sand loadings, rotating fluid bed behaviour at any superficial gas velocity tested during the experiments was not observed.

With an increase in the superficial gas velocity beyond the minimum fluidization velocity, the formation of jets and spouted fluidized bed behaviour was observed, as illustrated in Figure 4-7. This behaviour was likely due to the entrainment of fine solids contained in the sieved river sand at the start of each of the experiments. The entrainment reduced the large particle size distribution of the sieved river sand, resulting in the fluidized bed exhibiting Geldart D powder behaviour. Turbulent fluidization was also observed for all four river sand loadings at superficial gas velocities well above the minimum fluidization velocities.



**Figure 4-7:** Instantaneous snapshots of jet formation (3.5 kg river sand)

It was also observed that throughout the entire range of superficial gas velocities tested, there were regions of stationary river sand. These regions were located directly behind the air injectors, and remained relatively the same size throughout the experiments. All these observations imply that the centrifugal forces were significantly less than initially anticipated, and these regions of stationary bed material, causing non-uniform fluidization in the annulus, impede the momentum transfer between the moving air and river sand.

## 4.5 Alterations

In order to overcome the problems discussed in the previous section, and to achieve the desired induced rotating fluid bed behaviour in the annulus, several alternations to the assembled Perspex model were considered, namely:

- Increasing the velocity of the air by reducing the diameters of the air injectors;
- Delivering more air, either by installing an additional blower or a more powerful blower;
- Testing different materials of varying particle sizes and densities; and
- Considering a completely different air distribution system for the annulus.

#### 4.5.1 Reducing the Air Injector Diameter

It was hypothesized that a reduction in the air injector diameter could increase the momentum transfer between the moving air and river sand, potentially inducing the desired rotating fluid bed. Smaller diameter air injectors would deliver the fluidizing air at an increased velocity.

Based on the assumption that the momentum transfer of the moving air and river sand can be related to the dynamic pressure of the system, a relationship between the air injector diameter and momentum transfer could be established. Dynamic pressure ( $q$ ), defined as the kinetic energy per unit volume of a fluid particle, is calculated by multiplying its density ( $\rho$ ) by the square of its velocity ( $v$ ), and by a factor of 0.5 (Equation 4-1).

$$q = \frac{1}{2} \cdot \rho \cdot v^2 \quad (4-1)$$

Based on Equation 4-1, it is evident that the dynamic pressure, and therefore the momentum transfer, is proportional to the square of the air velocity. Since the velocity of the air is a function of the air injector dimensions, a minor reduction in the diameter could cause a significant increase in the momentum transfer between the moving air and river sand, as illustrated in Table 4-3.

**Table 4-3:** Influence of the air injector diameter on the momentum transfer at a constant superficial gas velocity of 0.5 m/s in the annulus

| Injector diameter          | 4 mm   | 4.5 mm | 5 mm   | 5.5 mm | 6 mm   | 6.5 mm |
|----------------------------|--------|--------|--------|--------|--------|--------|
| Injector air velocity      | 67 m/s | 53 m/s | 43 m/s | 35 m/s | 30 m/s | 25 m/s |
| Momentum transfer increase | 618 %  | 349 %  | 196 %  | 96 %   | 44 %   | -      |

The diameters of the copper pipes that were screwed into the air injector housings were reduced from 6.5 mm to 5 mm and the experiments were repeated. Unfortunately, even with an estimated 196% increase in the momentum transfer, no induced rotating fluid bed was observed throughout the entire range of the superficial gas velocities tested. Stationary regions of river sand located directly behind the air injectors were also still present.

#### 4.5.2 Installing an Additional Blower

It was also hypothesized that with the installation of an additional blower, more volume of air and higher superficial gas velocities in the annulus could be achieved, potentially resulting in an induced rotating fluid bed. Due to financial constraints, a second 1.75 kW blower could not be purchased, and instead an available 0.75 kW single-stage side-channel blower was used, connected in parallel. Both blowers were also rewired to be in the delta type ( $\Delta$ ) connection in order to increase the speed of the motors. In this type of connection, each phase receives the total line voltage as opposed to receiving only  $1/\sqrt{3}$  of the total line voltage in a star type (Y) connection. The experiments were repeated, and although the superficial gas velocity in each injector as well as in the annulus was increased, no rotation of the bed material was observed. Regions of stationary bed material were still present even when both blowers were operating at maximum power. It was therefore concluded that even with two blowers, there was still insufficient momentum transfer between the moving air and river sand to induce a rotating fluid bed.



### 4.5.3 Testing of Additional Materials

Four additional materials varying in particle sizes and bulk densities were tested in the annular fluidized bed in order to compare the observed results with those obtained with the river sand. Although none of the materials tested resulted in an induced rotating fluid bed, several key observations were made during the experiments. In the experiments conducted with ilmenite and the ilmenite-sand mixture, substantially more mass of bed material was required to evenly and sufficiently cover each air injector before the start of experiments. This was due to the fact that the ilmenite and ilmenite-sand samples had small volume average particle sizes (142  $\mu\text{m}$  and 165  $\mu\text{m}$  respectively) and high bulk densities (2 780  $\text{kg}/\text{m}^3$  and 2 230  $\text{kg}/\text{m}^3$  respectively). Figure 4-8 (*left*) depicts the depletion of bed material at several injectors using 3.0 kg of the ilmenite-sand mixture.



**Figure 4-8:** (*Left*) Depletion of bed material at several air injectors (3.0 kg ilmenite-sand mixture); (*right*) turbulent fluidization (4.0 kg ilmenite-sand mixture)

As the superficial gas velocity was gradually increased during the experiments conducted with ilmenite and the ilmenite-sand mixture, little bed expansion was observed, followed promptly by the formation of jets and turbulent fluidization (Figure 4-8 (*right*)). As with the observations described during the experiments conducted with the river sand, stationary regions of bed material located directly behind the air injectors were present throughout the entire range of superficial gas velocities tested.

In the experiments conducted with the mustard seeds, only spouted fluidized bed behaviour with minimal bed expansion was observed over the entire range of superficial gas velocities tested (Figure 4-9). These results could be expected since mustard seeds fall into the category of Geldart D type powders, which characteristically exhibit spouted fluidized bed behaviour. Large regions of stationary bed material located directly behind the air injectors were apparent, which did not reduce in size throughout the course of the experiments.

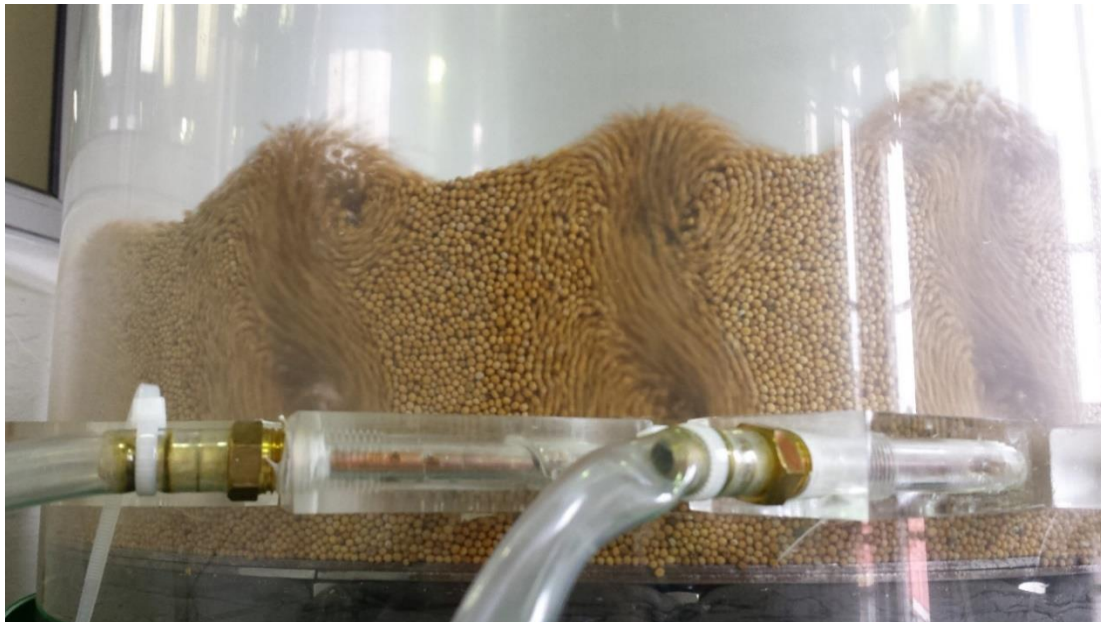


**Figure 4-9:** Spouted fluidized bed behaviour (1.5 kg mustard seeds)

In the experiments conducted using poppy seeds, bed expansion was visibly evident as the superficial gas velocity was gradually increased. It was determined that a

minimum of 1.0 kg of poppy seeds had to be charged into the annulus to ensure that each air injector was equally and sufficiently covered with bed material before the start of the experiments.

Three experiments were conducted using the poppy seeds: the poppy seed loading was increased from 1.0 kg to 2.0 kg in 0.5 kg increments. For each poppy seed loading charged into the annulus, the bed expansion was measured optically as the superficial gas velocity was gradually increased (Figure 4-10). Only the single 1.75 kW double-stage side-channel blower was connected to the Perspex setup, as with the results illustrated in Figure 4-6. The bed height and superficial gas velocity at minimum fluidization for each poppy seed loading is summarized in Table 4-4.

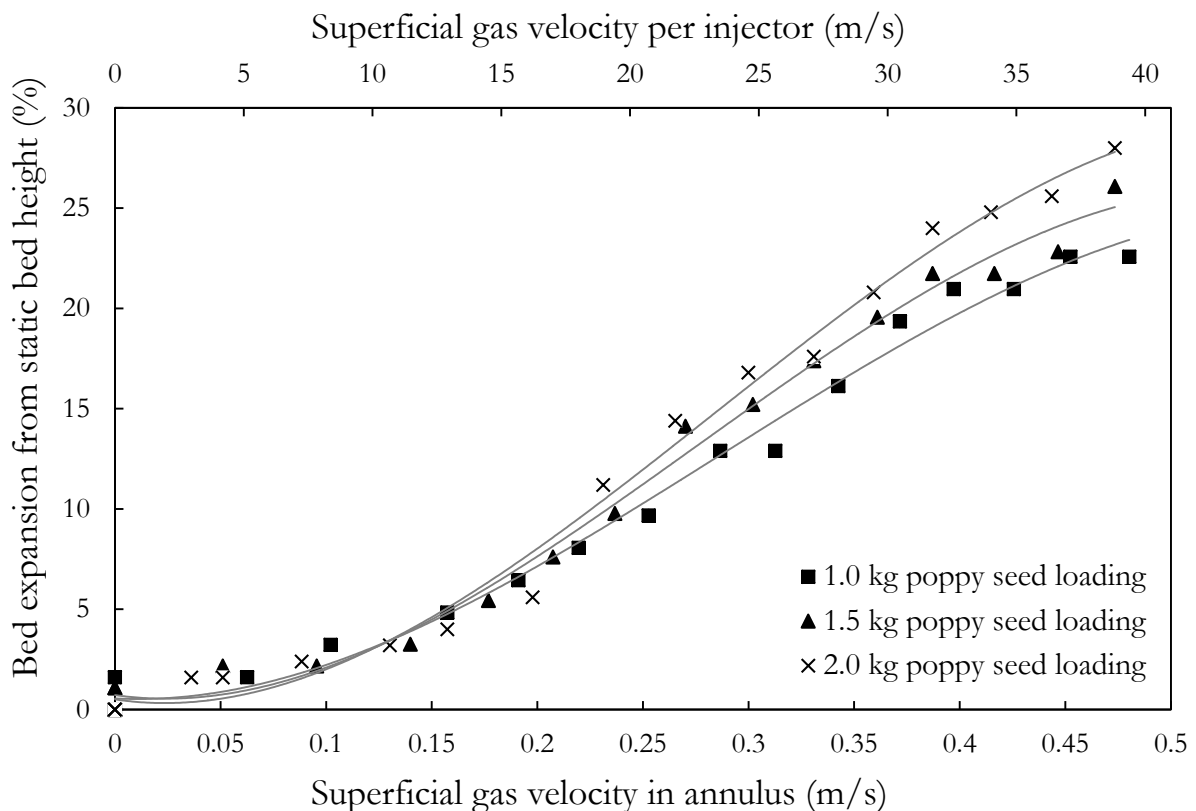


**Figure 4-10:** Comparison of bed expansion of poppy seeds from static bed height as a function of superficial gas velocity

In comparison with the results illustrated in Figure 4-6, at the same superficial gas velocity in the annulus the superficial gas velocity per injector in Figure 4-10 is



higher. This is due to the fact that the smaller diameter air injectors were used (5 mm as opposed to 6.5 mm), increasing the superficial gas velocities of the individual air injectors.

**Table 4-4:** Summary of poppy seed experimental results

|   | <b>Poppy seed loading</b> |        |        |
|---|---------------------------|--------|--------|
|   | 1.0 kg                    | 1.5 kg | 2.0 kg |
| <b>Static bed height (mm)</b>                           | 62                        | 92     | 125    |
| <b>Minimum fluidization velocity in annulus (m/s)</b>   | 0.07                      | 0.08   | 0.01   |
| <b>Bed height at minimum fluidization velocity (mm)</b> | 63                        | 94     | 128    |

As with the experimental results obtained with the river sand, the rate of bed expansion as well as the minimum fluidization velocity was determined to be proportional to the poppy seed loading. As the superficial gas velocity was increased beyond the minimum fluidization velocity, jet formation and spouted fluidized bed behaviour was observed (Figure 4-11 (*top*)).

Although some static charge was also observed (Figure 4-11 (*top*)), where several poppy seeds stuck to the inner walls of the annulus, it was determined that it had little significance to the overall results. As the superficial gas velocity increased well above the minimum fluidization velocity, turbulent fluidization was also observed (Figure 4-11 (*bottom*)).

Unfortunately, regions of stationary poppy seeds located directly behind the air injectors were also observed throughout the entire range of superficial gas velocities tested. As before, these observations imply that the centrifugal forces were significantly less than initially anticipated, and that these regions of stationary bed material, causing non-uniform fluidization in the annulus, impede the momentum transfer between the moving air and the poppy seeds.



**Figure 4-11:** (*Top*) Jet formation (1.0 kg poppy seeds); (*bottom*) turbulent fluidization (2.0 kg poppy seeds)

## 4.6 Conclusions and Recommendations

A physical model was constructed of two Perspex tubes which was used to study the behaviour of a fluidized bed in an annulus, testing various bed materials. It was hypothesized that by using multiple gas injectors orientated tangentially to the annulus walls, induced rotating fluid bed behaviour would occur in the annulus.

Unfortunately, even after a reduction in the air injector diameter and with the addition of a second blower, induced rotating fluid bed behaviour was not observed throughout the entire range of superficial gas velocities tested. Instead, as the superficial gas velocity increased beyond minimum fluidization, the formation of jets and spouted fluidized bed behaviour was observed, followed by turbulent fluidization. In experiments conducted with river sand and poppy seeds, it was found that with increasing superficial gas velocity, the rate of bed expansion was proportional to the bed material loading. Furthermore, the minimum fluidization velocity was also found to be proportional to the bed material loading. Regions of stationary bed material located directly behind the air injectors were also observed to be present for all materials tested.

Based on the above-mentioned observations, it was concluded that the centrifugal forces were significantly less than initially anticipated. Furthermore, it was concluded that the regions of stationary bed material cause non-uniform fluidization in the annulus. These regions impede the momentum transfer between the moving air and the bed material, preventing the possibility of any bed material rotation.

The consequence of these observations and the above-mentioned conclusions is that the design concept of using multiple air injectors orientated tangentially to the walls of the annular pyrolysis chamber will have to be modified to achieve uniform fluidization in the annulus. Should such a design be used in the new fluidized bed fast pyrolyser, multiple feed inlets would have to be located in close proximity to the gas injectors in order to ensure complete mixing and ensure sufficient time for reactions.

It is therefore recommended that a completely different air distributing system be designed for the annulus in order to overcome the difficulties experienced with the multiple tangential air injectors. Fixed angled blades, similar to the gas distributor

used in the TORBED reactor, is a promising design which is able to produce a swirling fluidized bed. Alternatively, a porous plate-type air distributor could be considered, which may possibly induce the desired rotating fluid bed behaviour by ensuring complete uniform fluidization in the annulus.

It is also recommended that a more detailed study, such as a dimensional analysis, should be performed in order to determine why these regions of stationary bed material occur and what impedes the momentum transfer. Ideally, after performing such an analysis, the parameters that have to be met in order to induce a rotating fluid bed behaviour in an annular fluidized bed could be established. Such information will be particularly useful in the event that the annular fluidized bed is scaled up.

---

# CHAPTER 5: ANGLED BLADES

---

A completely different air distributing system was designed to potentially overcome the difficulties experienced with the tangential air injectors described in Chapter 4. It was hypothesized that fixed angled blades, similar to the blades used in the gas distributor of the TORBED reactor, could induce a rotating fluid bed.

## 5.1 Design Concept

It was hypothesized that by using multiple overlapping metal leaves at fixed angles, induced rotating fluid bed behaviour would occur in the annulus. The fluidizing air would enter the bed at  $v$  m/s and at an angle  $\theta$  to the horizontal, and fluidization would occur due to the vertical component of the air velocity ( $v \sin \theta$ ), whereas the tangential component of the air velocity ( $v \cos \theta$ ) would cause rotation of the fluid bed. The momentum transfer between the moving air and bed of particles would therefore depend on the number of slits formed by the overlapping metal leaves, the angle of the slits, as well as the height of the slits. The linear velocity of the air entering the annulus through the slits would be determined by the slit dimensions.

## 5.2 Construction

A metal air distributor was manufactured from stainless steel with 32 spot-welded overlapping metal leaves, forming 32 slits. The height of each individual slit, and therefore the velocity of the air flowing out of the slit, could be adjusted by means of a screw located at the end of each metal leaf (Figure 5-1). The fluidizing air, flowing from the 16 tangential air injectors, could then be directed into the metal air distributor by means of 24 holes drilled into the base plate of the air distributor.

Thereafter the air would be redistributed to flow out from the slits formed by the overlapping metal leaves. In order to keep the metal air distributor in place, eight mounting bolts were used. The dimensions and specifications of the metal air distributor used in the Perspex model are summarised in Table 5-1. A photograph of the manufactured metal air distributor is shown in Figure 5-2.

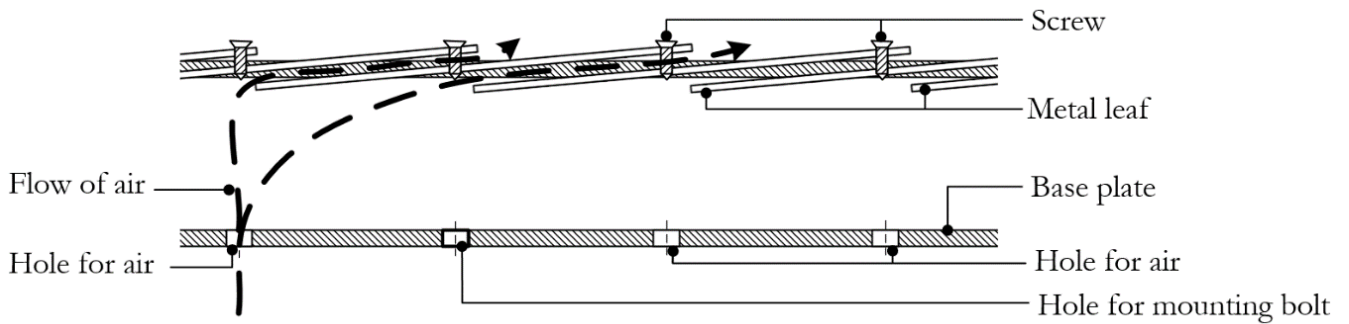


**Figure 5-1:** Detailed diagram of metal air distributor with overlapping metal leaves and adjustable screws

**Table 5-1:** Dimensions and specifications of the metal air distributor

| Specification                             | Value   | Units   |
|---|---|---------|
| Construction material                     | Stainless steel                                 | -       |
| Cross-sectional height of air distributor | $18 \times 10^{-3}$                             | m       |
| Cross-sectional width of air distributor  | $19 \times 10^{-3}$                             | m       |
| Base plate thickness                      | $3 \times 10^{-3}$                              | m       |
| Metal leaf thickness                      | $1 \times 10^{-3}$                              | m       |
| Wall thickness                            | $1 \times 10^{-3}$                              | m       |
| Number of metal leaves forming slits      | 32  | -       |
| Slit height                               | <i>Adjustable – specify for each experiment</i> |         |
| Slit length                               | $17 \times 10^{-3}$                             | m       |
| Slit angle                                | 10  | degrees |
| Number of holes for fluidizing air        | 24  | -       |
| Diameter of holes for fluidizing air      | $7 \times 10^{-3}$                              | m       |
| Number of holes for mounting bolts        | 8   | -       |





**Figure 5-2:** Photograph of the metal air distributor

### 5.3 Initial Experiments

In order to determine the desired height that the slits should be adjusted to, a comparison of the total cross-sectional areas and linear air velocities was made between the copper pipes used in Chapter 4 and overlapping metal leaves (Table 5-2). For the sake of comparison, a slit height of 0.5 mm was selected, yielding an air velocity of 49 m/s, similar to the 43 m/s delivered by the 5 mm inner diameter copper pipes used as the tangential air injectors.

As with the initial experiments conducted with the tangential air injectors in the Perspex model, the superficial gas velocity was gradually increased using the variable speed controller with no bed material in the annulus. This test was performed in order to ensure that the 1.75 kW double-stage side-channel blower was operating properly, all 16 gas injectors were delivering the fluidizing air to the metal air distributor and that no air leaks could be detected outside of the annulus. In order to check that the fluidizing air flowing from the multiple tangential air injectors was

indeed directed into the holes drilled into the base plate and out from the slits of the metal air distributor, 0.5 kg of mustard seeds were loaded into the annulus. Mustard seeds were selected as the preferred material for this test as the particle size of the individual seeds was significantly greater than the slit height of 0.5 mm, which guaranteed that no seeds could obstruct the slits and possibly impede the flow of air.

**Table 5-2:** Comparison of cross-sectional areas using various air injectors at a constant superficial gas velocity of 0.5 m/s in the annulus

|                                    | Cross-sectional<br>area per<br>injector/leaf (m <sup>2</sup> ) | Total cross-<br>sectional area<br>(m <sup>2</sup> ) | Injector/leaf<br>air velocity<br>(m/s) |
|------------------------------------|--|---|--|
| <b>16 copper pipes</b>             |  |   |  |
| Inner diameter of 6.5 mm           | 3.32 x 10 <sup>-5</sup>  | 5.31 x 10 <sup>-4</sup>                             | 25                                     |
| Inner diameter of 5 mm             | 1.96 x 10 <sup>-5</sup>  | 3.14 x 10 <sup>-4</sup>                             | 43                                     |
| <b>32 overlapping metal leaves</b> |  |   |  |
| Slit height of 2 mm                | 3.4 x 10 <sup>-5</sup>   | 1.09 x 10 <sup>-3</sup>                             | 12                                     |
| Slit height of 1 mm                | 1.7 x 10 <sup>-5</sup>   | 5.44 x 10 <sup>-4</sup>                             | 25                                     |
| Slit height of 0.5 mm              | 8.5 x 10 <sup>-6</sup>   | 2.72 x 10 <sup>-4</sup>                             | 49                                     |
| Slit height of 0.3 mm              | 5.1 x 10 <sup>-6</sup>   | 1.63 x 10 <sup>-4</sup>                             | 82                                     |
| Slit height of 0.1 mm              | 1.7 x 10 <sup>-6</sup>   | 5.44 x 10 <sup>-5</sup>                             | 246                                    |

Due to the fact that the two Perspex tubes were not completely concentric, seepage of the fluidizing air along the inner walls of the annulus, as opposed to the air flowing through the overlapping metal leaves, was observed (Figure 5-3). In addition, since the overlapping metal leaves were not welded to the walls of the metal air distributor, poor fluidization was anticipated for future experiments. In order to overcome these problems, all the gaps from which the fluidizing air could escape were sealed with latex gum, and the outer walls of the metal air distributor were ground down to a smooth finish and lined with tape to ensure an airtight fit in the annulus.





**Figure 5-3:** Seepage of fluidizing air along the inner walls of the Perspex tubes (0.5 kg mustard seeds)

During these initial experiments, it was also determined that before the start of the experiments, the slit height of each individual slit had to be carefully and precisely adjusted to exactly the specified slit height. This is because a minor difference in the height of even one slit could lead to an uneven pressure drop and an uneven distribution of air in the metal distributor, resulting in non-uniform fluidization in the annulus.

## 5.4 Results and Discussion

Controlled amounts of river sand, ilmenite, an ilmenite-sand mixture, mustard seeds and poppy seeds were then sequentially loaded into the annulus and observations were made as the superficial gas velocity was gradually increased. If very little bed material was charged into the annulus and the slits were only just covered, the bed material at some slits would be completely removed, resulting in an uneven pressure drop and uneven air distribution in the distributor. The removed bed material was

initially suspended and swirled around the annulus in a manner similar to pneumatic conveying. Bed material inevitably accumulated on top of other slits and the suspended bed material eventually settled on the build-up. To recapitulate, similar observations were made with the Perspex model using multiple tangential injectors (Figure 4-4). The uneven pressure drop and uneven air distribution was also exacerbated by minute differences in slit heights and some seepage of air along the inner walls of the annulus was still apparent.

Over the entire range of superficial gas velocities tested, with various slit heights of 0.5 mm, 0.4 mm and 0.3 mm, induced rotating fluid bed behaviour was unfortunately not observed for any of the materials tested. As with the observations described in Chapter 4, jet formation and spouted fluidized bed behaviour was observed as the superficial gas velocity was gradually increased, followed by turbulent fluidization (Figure 5-4). These observations imply that the components of the air velocity, both vertical and tangential ( $v \sin \theta$  and  $v \cos \theta$ ), flowing through the slits were insufficient to result in uniform fluidization or the desired induced rotating bed behaviour. Stationary regions of bed material, located on top of the overlapping metal leaves, were also observed but were significantly smaller in size compared to the same regions observed directly behind the air injectors (refer to Chapter 4). It was concluded that the reduction in the size of these regions was a direct consequence of using 32 slits, which ensured more uniform fluidization in the annulus. Using more than 32 slits could potentially eliminate the regions of stationary bed material altogether.

Interestingly, in experiments conducted with river sand and poppy seeds, the fluidized bed in the annulus seemed to give the impression that it was rotating slightly in the opposite direction to the slits at the maximum blower settings (superficial gas velocity of 0.5 m/s in the annulus). Even with the addition of the 0.75 kW single-stage side-channel blower, the same phenomenon was observed.

Although initially it was thought that this observation was an optical illusion, it was later concluded that the fluidizing air was forming eddies as it impacted on regions of stationary bed material, pushing the fluidized air and fluidized bed material in the opposite direction. This observation supported the previously drawn conclusion that momentum transfer between the moving air and bed material was impeded by the stationary regions of bed material, preventing any induced rotating fluid bed behaviour in the annulus. Completely eliminating these regions could potentially result in an induced rotating fluid bed.

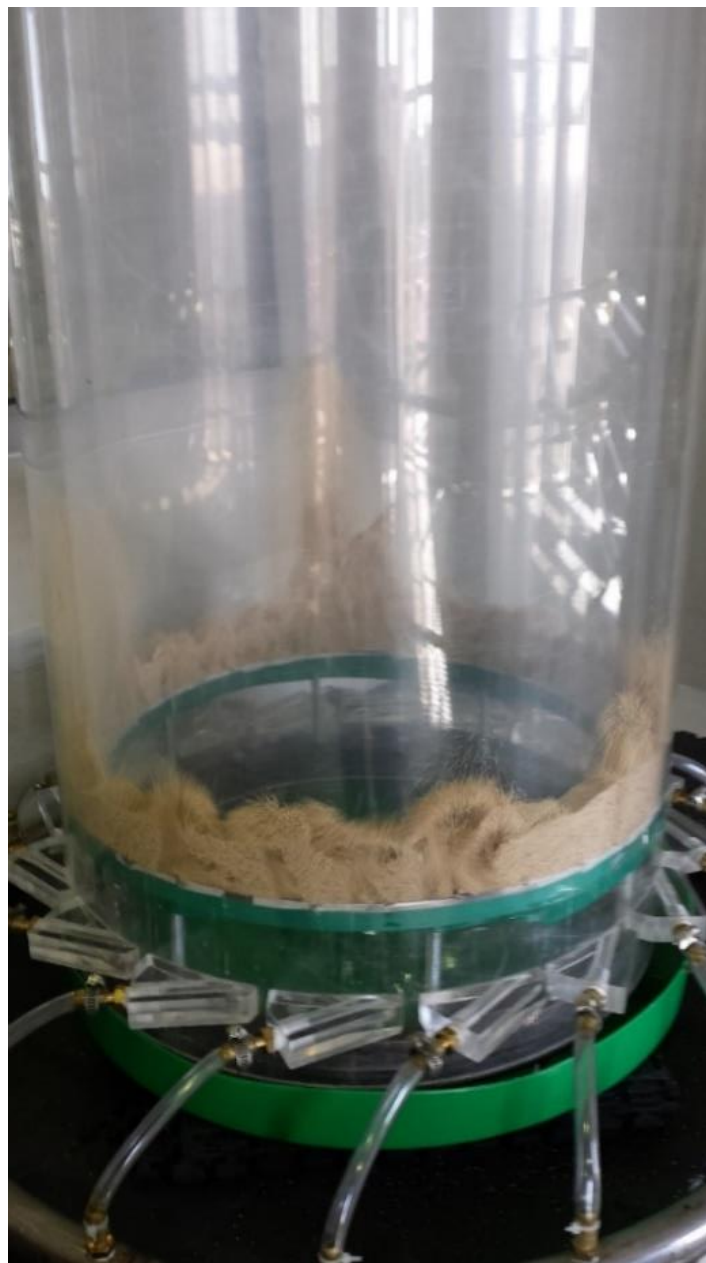


**Figure 5-4:** Turbulent fluidization behaviour (0.5 kg poppy seeds)

## 5.5 Alterations

In order to overcome the problems discussed in the previous section, and in order to achieve the desired induced rotating fluid bed behaviour in the annulus, several alterations were considered, namely:

- Manufacturing a more airtight air distributor;
- Increasing the number of slits to achieve uniform fluidization;
- Considering a porous plate-type air distributor; and
- Conducting a dimensional analysis to determine the parameters that should be met in order to induce rotating fluid bed behaviour in the annulus.

### 5.5.1 Increasing the Number of Slits

The regions of stationary bed material located on top of the overlapping leaves could potentially be completely eliminated by using more slits ( $>32$  slits). With the addition of more slits, the floor of the annulus would be more uniformly fluidized, possibly resulting in induced rotating fluid bed behaviour. It was hypothesized that doubling the number of slits from 32 to 64 would suffice as the additional slits would be located at the centre of the regions of stationary bed material. However, as the overlapping metal leaves in the metal air distributor had been spot-welded into position, a new air distributor would have had to be designed and manufactured. That being said, a metal air distributor with 64 height-adjustable overlapping metal leaves was deemed physically unrealisable to manufacture from stainless steel due to the difficulty of achieving the close tolerances required to ensure an airtight fit in the annulus and the necessity to adjust precise slit heights.

For the above-mentioned reasons, it was decided that the new air distributor should be 3-dimensionally printed using polylactic acid (PLA). Although the 3D printed air distributor would not have height-adjustable slits, it was anticipated that the accuracy

of the printing process would ensure uniform fluidization in the annulus since each slit would be printed to exactly the same slit height.

The 3D printed air distributor was designed to have 64 slits with slit heights of 0.5 mm at 45° – double the percentage open area of the metal air distributor described in the previous section. In order to minimize any seepage of the fluidizing air along the inner walls of the annulus, the 3D printed air distributor was designed to be trapezoidal in cross-section, where the base plate of the air distributor was slightly wider than the top plate containing the slits. The fluidizing air flowing from the tapped holes in the rolled pipe was directed to the air injector holes located on the base plate of the air distributor by means of silicon tubing. A detailed diagram of the 3D printed PLA air distributor is illustrated in Figure 5-5.

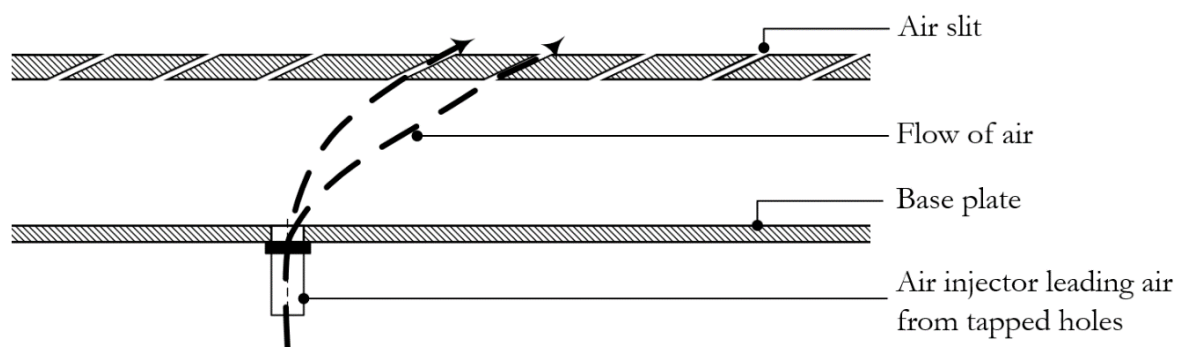


**Figure 5-5:** Detailed diagram of 3D printed PLA air distributor

As with all the initial experiments described in previous sections, the superficial gas velocity was gradually increased using the variable speed controller with no bed material in the annulus. This test was performed in order to ensure that the 1.75 kW double-stage side-channel blower was operating properly, all tapped holes were delivering the fluidizing air directly into the 3D printed air distributor and that no air leaks could be detected outside of the annulus. Thereafter controlled amounts of river sand, ilmenite, the ilmenite-sand mixture, mustard seeds and poppy seeds were sequentially loaded into the annulus, and observations were made as the superficial gas velocity was gradually increased. Although induced rotating fluid bed behaviour



was, once again, not observed with any of the materials tested using the 1.75 kW blower, as well as with the addition of the 0.75 kW blower, several key observations were made during the experiments.

Bubbling fluidization was observed during the experiments conducted with the river sand and poppy seeds at superficial gas velocities of 0.3 m/s and 0.26 m/s in the annulus respectively (Figure 5-6). As the superficial gas velocity was increased beyond the bubbling fluidization velocity, turbulent fluidization followed. In comparison to the experiments performed with the river sand and poppy seeds described previously using the multiple tangential air injectors and the overlapping metal leaves, the fact that bubbling fluidization was observed is unique. This observation supported the hypothesis that increasing the number of slits could result in more uniform fluidization in the annulus, significantly improving the mixing effects of the bed material.



**Figure 5-6:** Bubbling fluidization behaviour (0.5 kg poppy seeds)

To recapitulate, uniform fluidization in the annulus relates directly to an even pressure drop and an even distribution of air in the air distributor. For these reasons, it was concluded that the vertical component of the velocity flowing through the

slits was sufficient to achieve uniform bubbling fluidization, but the tangential component of the velocity was insufficient to induce any rotation of the fluid bed.

Bubbling fluidization was not observed during any of the experiments conducted using ilmenite, the ilmenite-sand mixture or the mustard seeds. Several slits in the air distributor were blocked by the particles of the ilmenite and ilmenite-sand mixture, resulting in non-uniform fluidization in the annulus. A reduction in the slit height may resolve this problem. In experiments conducted with mustard seeds, only spouted fluidization with minimal bed expansion was observed over the entire range of superficial gas velocities tested.

In order to determine the ideal air distributor design for the annulus, which would ensure uniform fluidization as well as induced rotating fluid bed behaviour, it is recommended that experiments should be repeated with varying numbers of slits, slit angles and slit heights. However, it has already been mentioned that manufacturing this type of air distributor from stainless steel, or any other material that can withstand pyrolysis temperatures ( $\pm 500$  °C), is physically unrealisable. For this reason, a porous plate-type air distributor should be considered as an alternative. Porous plate-type distributors are known to provide good fluidization, and if manufactured from ceramic materials, would also be more practical for the annular pyrolysis chamber in the new fluidized bed fast pyrolyser.

### **5.5.2 Independent Research**

Independent research relevant to this dissertation, conducted at the Pyrolysis Laboratories of the Department of Chemical Engineering at the University of Pretoria, was also analysed to assist in the understanding of the hydrodynamic behaviour of the annular fluidized bed. Airaga (2015) used a bench-scale experimental apparatus to study the viscosity effects in fluidized beds. It was



demonstrated that the viscosity of the bed material in a fluidized bed decreased as the superficial gas velocity increased (Airaga, 2015). In addition, Airaga (2015) also demonstrated that the viscosity of the bed material remained constant at superficial gas velocities above 0.7 m/s, as illustrated in Figure 5-7.

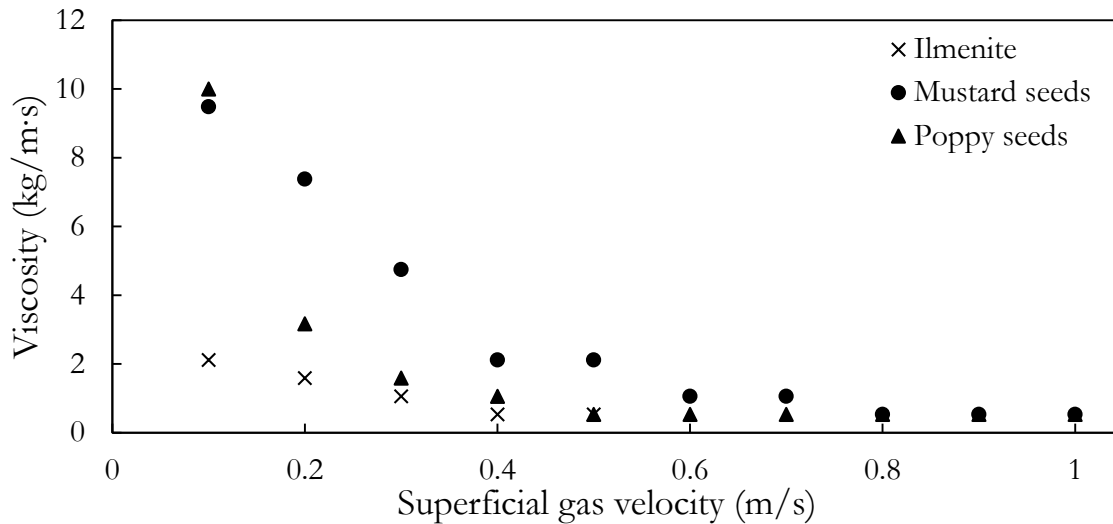


**Figure 5-7:** Viscosity for various bed materials as a function of superficial gas velocity (adapted from Airaga, 2015)

It can therefore be concluded from Figure 5-7 that the viscosity of the bed material and the superficial gas velocity and are inversely proportional up until 0.7 m/s. Since the viscosity of any material relates to the resistance to flow and/or movement, the results in Figure 5-7 indicate that at low superficial gas velocities, the resistance to flow and/or movement of the bed material is high. Conversely, the resistance to flow and/or movement of the bed material is low at high superficial gas velocities. These results are justified because as increasing amounts of fluidizing gas percolate through the void spaces between the particles of the bed material, the bulk density of the bed decreases, which in turn reduces the resistance to flow and/or movement.

Relating the above-mentioned results to the research presented in this dissertation, it can be concluded that the regions of stationary bed material previously described had a high viscosity and therefore a high resistance to flow and/or movement. These regions of high viscosity forced the moving air vertically upwards, where the

viscosity was low, resulting in the formation of jets and spouted fluidized bed behaviour. It was therefore concluded that uniformly fluidizing the bed material in the annulus will ensure the same viscosity throughout the bed material with minimal resistance to flow and/or movement.

It is therefore recommended that since high superficial gas velocities are required for all the bed material to reach a minimum viscosity, a more powerful blower, able to reach higher than 0.7 m/s in the annulus, should be tested as it may result in an induced rotating fluid bed. It is then also recommended that a study should be performed in order to check whether sufficient contact time is available for the pyrolysis reactions to occur at such high superficial gas velocities. If not, the design concept of an induced rotating fluid bed in the annular pyrolysis chamber of the new fluidized bed fast pyrolyser could be impractical. In such an event, a rotating gas distributor plate should be considered instead.

### **5.5.3 Dimensional Analysis**

In order to determine the parameters that should be met in order to induce a rotating fluid bed in the annulus, a dimensional analysis was performed using Microsoft Excel®. Based on the fact that the slit-type air distributor described in this chapter presented the most promising results, sensitivity studies were performed on designs of this type of air distributor.

In order to determine what other air distributor configurations could result in uniform fluidization, a sensitivity study was performed where the dimensions of the slits, or alternatively holes, in the floor of the air distributor varied. Since uniform fluidization was observed with the 3D printed air distributor, which had slit widths of 13 mm and slit heights of 0.5 mm, the percentage open area of this air distributor design of 1.6% was chosen as the basis. Theoretically, a percentage open area of

1.6% can be achieved using a variety of configurations, which are illustrated in Table 5-3.

**Table 5-3:** Comparison of slit and hole dimensions and numbers to achieve a percentage open area of at least 1.6%

| <b>Rectangular slits widths of 13 mm in a slit-type air distributor</b> |                         |                        |
|---|-------------------------|------------------------|
| <i>Slit height</i>  | <i>Slit area</i>        | <i>Number of slits</i> |
| 0.1 mm  | 1.3 mm <sup>2</sup>     | 321                    |
| 0.2 mm  | 2.6 mm <sup>2</sup>     | 160                    |
| 0.3 mm  | 3.9 mm <sup>2</sup>     | 107                    |
| 0.4 mm  | 5.2 mm <sup>2</sup>     | 80                     |
| 0.5 mm  | 6.5 mm <sup>2</sup>     | 64                     |
| 0.6 mm  | 7.8 mm <sup>2</sup>     | 53                     |
| 0.7 mm  | 9.1 mm <sup>2</sup>     | 46                     |
| 0.8 mm  | 10.4 mm <sup>2</sup>    | 40                     |
| 0.9 mm  | 11.7 mm <sup>2</sup>    | 36                     |
| 1.0 mm  | 13 mm <sup>2</sup>      | 32                     |
| <b>Circular holes in a porous plate-type air distributor</b>            |                         |                        |
| <i>Hole diameter</i>  | <i>Hole area</i>        | <i>Number of holes</i> |
| 0.1 mm  | 0.00785 mm <sup>2</sup> | 53 115                 |
| 0.2 mm  | 0.0314 mm <sup>2</sup>  | 13 279                 |
| 0.3 mm  | 0.07065 mm <sup>2</sup> | 5 902                  |
| 0.4 mm  | 0.1256 mm <sup>2</sup>  | 3 320                  |
| 0.5 mm  | 0.19625 mm <sup>2</sup> | 2 125                  |
| 0.6 mm  | 0.2826 mm <sup>2</sup>  | 1 475                  |
| 0.7 mm  | 0.38465 mm <sup>2</sup> | 1 084                  |
| 0.8 mm  | 0.5024 mm <sup>2</sup>  | 830                    |
| 0.9 mm  | 0.63585 mm <sup>2</sup> | 656                    |
| 1.0 mm  | 0.785 mm <sup>2</sup>   | 531                    |

Based on the results in Table 5-3, it is evident that with smaller slit heights and smaller hole diameters, the number of slits and holes required to achieve the minimum percentage open area increases. Although a percentage free area of 1.6% for all rectangular slits and circular holes in Table 5-3 is attained, the rectangular slits with slit heights larger than 0.6 mm are not recommended for future air distributor designs because of the possibility of regions of stationary bed material. Conversely, very small slit heights and hole diameters are also not recommended as manufacturing these types of air distributors for the annular pyrolysis chamber could be problematic. As previously mentioned, manufacturing a slit-type air distributor from stainless steel, or any other material that can withstand pyrolysis temperatures ( $\pm 500$  °C), is physically unrealisable. Therefore it is recommended that future experiments should rather test porous plate-type air distributors with varying numbers of holes, hole angles and hole diameters.

A second sensitivity study investigated the effect of the slit angle on the superficial gas velocity required for uniform fluidization in the annulus. It was previously concluded that the vertical component of the velocity flowing through the slits of the 3D printed air distributor was sufficient to achieve uniform fluidization in experiments conducted using river sand and poppy seeds. At a superficial gas velocity of 0.3 m/s in the annulus, the velocity of the fluidizing air flowing out of each slit was calculated to be approximately 19 m/s, and at a slit angle of 45°, the vertical and tangential components were calculated to both be 13.5 m/s. Based on the assumption that uniform fluidization can be achieved if the vertical component of the fluidizing air flowing out of each slit is at least 13.5 m/s, a comparison of the minimum superficial gas velocity required to achieve uniform fluidization in the annulus as a function of the slit angle was made (Figure 5-8).

As the slit angle reduces from 90° (perpendicular to the horizontal) to 0° (parallel to the horizontal), the superficial gas velocity in the annulus required to achieve

uniform bubbling fluidization increases exponentially. In addition, since the vertical component of the velocity flowing out of the slit is constant at 13.5 m/s, the tangential component of the velocity flowing out of each slit also increases exponentially as the slit angle approaches 0°.

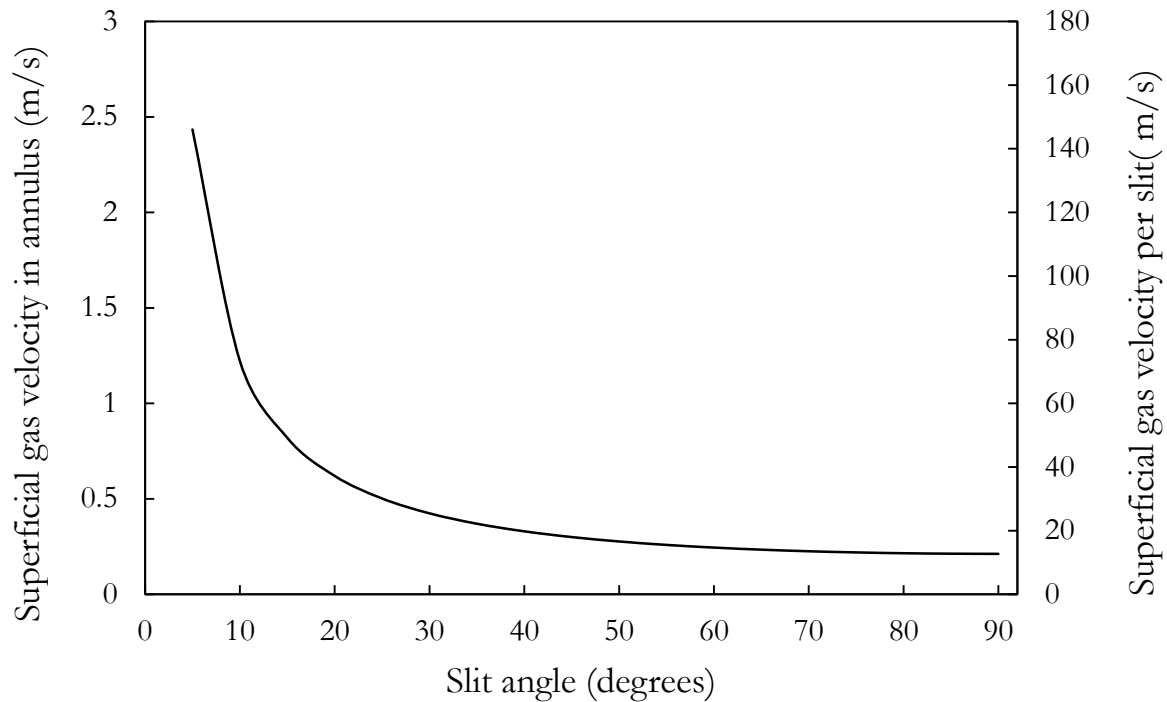


**Figure 5-8:** Superficial gas velocity in annulus required to achieve uniform bubbling fluidization as a function of the slit angle (slit dimensions: 13 mm x 0.5 mm, 64 slits)

It was now hypothesized that once uniform fluidization is achieved, induced rotating fluid bed behaviour is likely to occur with sufficient fluidizing air flowing in the tangential direction since the bed material experiences little resistance to flow and/or movement. In order to test this hypothesis, it is recommended that future experiments should be conducted using slit (or hole) angles below 45° and with blowers able to achieve higher superficial gas velocities in the annulus (>1 m/s). However, it has already been mentioned that in such an event, it is then also recommended that a study should be performed in order to check whether sufficient contact time is available for the pyrolysis reactions to occur at such high superficial gas velocities. If not, the design concept of an induced rotating fluid bed in the

annular pyrolysis chamber of the new fluidized bed fast pyrolyser could be impractical. In such an event, a rotating gas distributor plate should be considered instead.

## 5.6 Conclusions and Recommendations

A completely different air distributing system was designed to potentially overcome the difficulties experienced with the multiple tangential air injectors described in Chapter 4. It was hypothesized that fixed angled blades, similar to the blades used in the gas distributor of the TORBED reactor, could induce rotating fluid bed behaviour.

A metal air distributor was designed and manufactured from stainless steel to have 32 overlapping metal leaves. The height of each individual slit could be adjusted by means of a screw located at the end of each metal leaf. Unfortunately, over the entire range of superficial gas velocities tested and with various slit heights, induced rotating fluid bed behaviour was not observed for any of the bed materials tested. As with the observations described in Chapter 4, jet formation and spouted fluidized bed behaviour was observed as the superficial gas velocity was gradually increased, followed by turbulent fluidization. Stationary regions of bed material, located on top of the overlapping metal leaves, were also observed but were significantly smaller in size compared to the regions observed directly behind the tangential air injectors. Based on these observations, it was concluded that the vertical and tangential components ( $v \sin\theta$  and  $v \cos\theta$ ) of the air velocity flowing through the overlapping metal leaves were insufficient to result in uniform fluidization or the desired induced rotating bed behaviour.

In order to overcome the problems experienced with the metal air distributor, a new 3D printed air distributor was designed and manufactured from polylactic acid

(PLA). The 3D printed air distributor was designed to have 64 slits with fixed slit heights of 0.5 mm at 45° angles. Although induced rotating fluid bed behaviour was once again not observed with any of the materials at any of the superficial gas velocities tested, uniform bubbling fluidization was observed during experiments conducted using river sand and poppy seeds. This observation indicated that the vertical component ( $v \sin\theta$ ) of the velocity flowing through the slits was sufficient to achieve uniform fluidization in the annulus which significantly increased the mixing effects of the bed material. However, the tangential component ( $v \cos\theta$ ) of the velocity was still insufficient to induce any rotation of the fluid bed.

From independent research conducted at the Pyrolysis Laboratories in the Department of Chemical Engineering at the University of Pretoria, it was concluded that the regions of stationary bed material previously described had a high viscosity and therefore a high resistance to flow and/or movement. As the fluidizing air impacted on these regions of high viscosity, the moving air was forced vertically upwards, resulting in the formation of jets and spouted fluidized bed behaviour. It was therefore concluded that for induced rotating fluid bed behaviour to occur, it is essential that the entire floor of the annulus first be uniformly fluidized, ensuring the same viscosity throughout the bed material with minimal resistance to flow and/or movement.

Based on the sensitivity studies performed, a minimum percentage open area of 1.6% was recommended to ensure uniform fluidization of the bed material in the annulus. Since manufacturing slit-type air distributors with many slits and precise slit heights was deemed physically unrealisable, future experiments should rather test porous plate-type air distributors. Porous plate-type distributors are known to provide good fluidization, and if manufactured from ceramic materials, would also be more practical for the annular pyrolysis chamber in the new fluidized bed fast pyrolyser.



It was also hypothesized that once uniform fluidization is achieved, induced rotating fluid bed behaviour is likely to occur with sufficient fluidizing air flowing in the tangential direction since the bed material experiences little resistance to flow and/or movement. In order to test this hypothesis, it is recommended that future experiments should be conducted using slit (or hole) angles below  $45^\circ$  and with blowers able to achieve higher superficial gas velocities in the annulus ( $>1$  m/s).

If more powerful blowers are tested in future experiments, it is also recommended that a study should be done to check whether sufficient contact time is available for the pyrolysis reactions to occur at such high superficial gas velocities. If not, the design concept of an induced rotating fluid bed in the annular pyrolysis chamber of the new fluidized bed fast pyrolyser could be impractical. In such an event, a rotating gas distributor plate should be considered instead.

## 5.7 Reference

Airaga, EM (2015) “Viscosity effects in fluidized beds”, CSC 411 Report, Department of Chemical Engineering, University of Pretoria, South Africa.

---

# CHAPTER 6: CFD SIMULATIONS

---

In order to study the hydrodynamic behaviour of the annular fluidized bed in more detail, representative 2-dimensional CFD models were simulated using the Euler-Euler Model – Laminar Flow Interface in COMSOL Multiphysics® software. The Euler-Euler Model – Laminar Flow Interface is suitable to simulate the flow of two continuous and fully interpenetrating incompressible phases at low to moderate Reynolds numbers. This model can handle large differences in density between phases, making it ideal to simulate solid particles in gas and in liquid, as well as the transportation of liquid droplets or bubbles in a liquid.

## 6.1 The Euler-Euler Model

In order to calculate the velocity field for each phase, the model solves two sets of Navier-Stokes equations. The interphase momentum transfer,  $\mathbf{F}$ , between the continuous phase and the dispersed phase is described by Equation 6-1. The subscript  $c$  denotes quantities relating to the continuous phase (air), whereas the subscript  $d$  denotes quantities relating to the dispersed phase (bed material). Based on the assumption that the interphase momentum transfer is dominated by the drag force, the drag acting on each phase can be further described by a drag force coefficient,  $\beta$ . The slip velocity,  $\mathbf{u}_{slip}$ , is defined by Equation 6-2, where  $\mathbf{u}$  is the velocity of each phase.

$$\mathbf{F}_{drag,c} = -\mathbf{F}_{drag,d} = \beta \mathbf{u}_{slip} \quad (6-1)$$

$$\mathbf{u}_{slip} = \mathbf{u}_d - \mathbf{u}_c \quad (6-2)$$

In all the simulations, the Gidaspow drag model was used (Equation 6-3), where  $\varphi$  denotes the phase volume fraction,  $\rho$  is the density,  $C_{drag}$  is the drag coefficient for a single dispersed particle,  $d$  is the dispersed phase particle diameter and  $\mu$  is the dynamic viscosity.

$$\beta = \frac{3\varphi_c\varphi_d\rho_c C_{drag}}{4d_d} [\mathbf{u}_{slip}] \varphi_c^{-2.65} \text{ for } \varphi_c > 0.8$$

$$\beta = 150 \frac{\mu_c \varphi_d^2}{\varphi_c d_d^2} + 1.75 \frac{\varphi_d \rho_c}{d_d} [\mathbf{u}_{slip}] \text{ for } \varphi_c < 0.8$$
(6-3)

A solid pressure model,  $p_s$ , is also required to model the particle-particle interactions and collisions as well as the friction experienced between two particles. In all the simulations, the Gidaspow-Ettechadieh model was used, as described in Equation 6-4.

$$\nabla p_s = -10^{-8.76\varphi_c + 5.43} \nabla \varphi_c$$
(6-4)

Along the wall boundaries, a slip condition for the dispersed phase, and a non-slip condition for the continuous phase, were applied. Physics-controlled meshes were generated for each individual simulation, ensuring a finer meshing sequence along the boundaries and inlets, resulting in more accurate solutions. Although induced rotating fluid bed behaviour was unfortunately not observed during any of the simulations, the results still proved beneficial as they could illustrate several hydrodynamic properties not visibly obvious in the experiments conducted with the Perspex model.

## 6.2 Tangential Injectors

In order to reduce the computational time, only a section of the annulus was modelled on a 2D surface, as illustrated in Figure 6-1. Five square injector inlets

( $inlH$ ), representative of five air injectors in the Perspex model, were equally spaced out along the bed width ( $bedW$ ). The initial dispersed phase height ( $solidH0$ ) varied, depending on the bed material loading simulated. An outlet boundary was located at the top of the geometry, at bed height ( $bedH$ ), which allowed for the rising air to escape. The parameters which remained constant in all the CFD models of the tangential injectors are listed in Table 6-1.

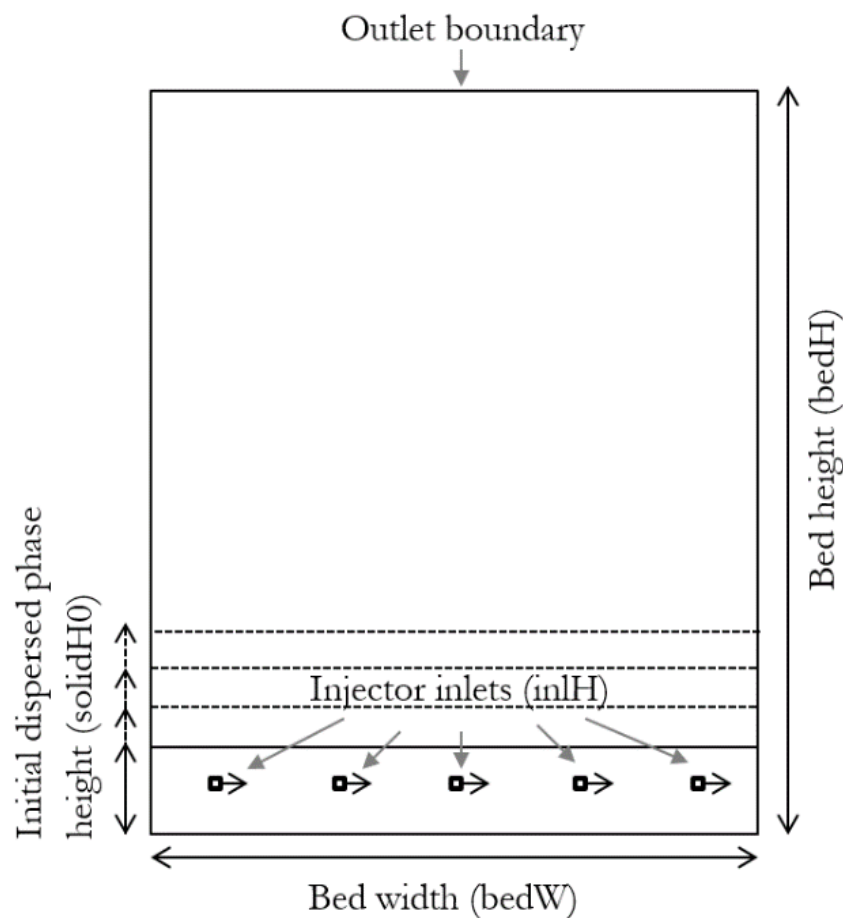


**Figure 6-1:** Geometry of the CFD models of the tangential injectors

As with the experiments conducted using the Perspex model, the primary material tested with the CFD models was river sand. The results for the 2.5 kg river sand loading are discussed in detail in the following section, and a general conclusion is drawn for the remaining river sand loadings. A brief discussion is also included on the additional materials simulated using the CFD model of the tangential injectors.

**Table 6-1:** Parameters for the CFD models of the tangential injectors

| Parameter | Description                             | Value                            | Units             |
|-----------|---|----------------------------------|-------------------|
| bedH      | Fluidized bed height                    | 0.5                              | m                 |
| bedW      | Fluidized bed width                     | 0.44                             | m                 |
| diam      | Particle size of dispersed phase        | <i>Specify for each material</i> |                   |
| inlH      | Injector size                           | $6.5 \times 10^{-3}$             | m                 |
| muc       | Dynamic viscosity of continuous phase   | $1.8 \times 10^{-5}$             | Pa·s              |
| phid0     | Initial dispersed phase volume fraction | <i>Specify for each material</i> |                   |
| rhoc      | Continuous phase density                | 1.2                              | kg/m <sup>3</sup> |
| rhod      | Dispersed phase density                 | <i>Specify for each material</i> |                   |
| solidH0   | Initial dispersed phase height          | <i>Specify for each material</i> |                   |

### 6.2.1 River Sand

The material-specific parameters used in the 2.5 kg river sand loading simulation are listed in Table 6-2. The physics-controlled mesh generated for the geometry used in the simulation comprised 25 415 triangular elements and 924 quadrilateral elements.

**Table 6-2:** Material-specific parameters used in the 2.5 kg river sand loading simulation

| Parameter | Description                             | Value                | Units             |
|-----------|---|----------------------|-------------------|
| diam      | Particle size of dispersed phase        | $5 \times 10^{-4}$   | m                 |
| phid0     | Initial dispersed phase volume fraction | 0.65                 |                   |
| rhod      | Dispersed phase density                 | 2070                 | kg/m <sup>3</sup> |
| solidH0   | Initial dispersed phase height          | $6.5 \times 10^{-2}$ | m                 |

The simulation was studied over a period of 5 seconds, ensuring sufficient time for the CFD model to reach a pseudo-steady state. The results from the simulation, depicting how the dispersed phase volume fraction changes over time, are illustrated

in a series of instantaneous snapshots in Figure 6-2. In comparison to the observed Perspex model results discussed in Chapter 4, the simulation results illustrated in Figure 6-2 slightly over-predicted the bed expansion of the river sand from the static bed height of 65 mm.

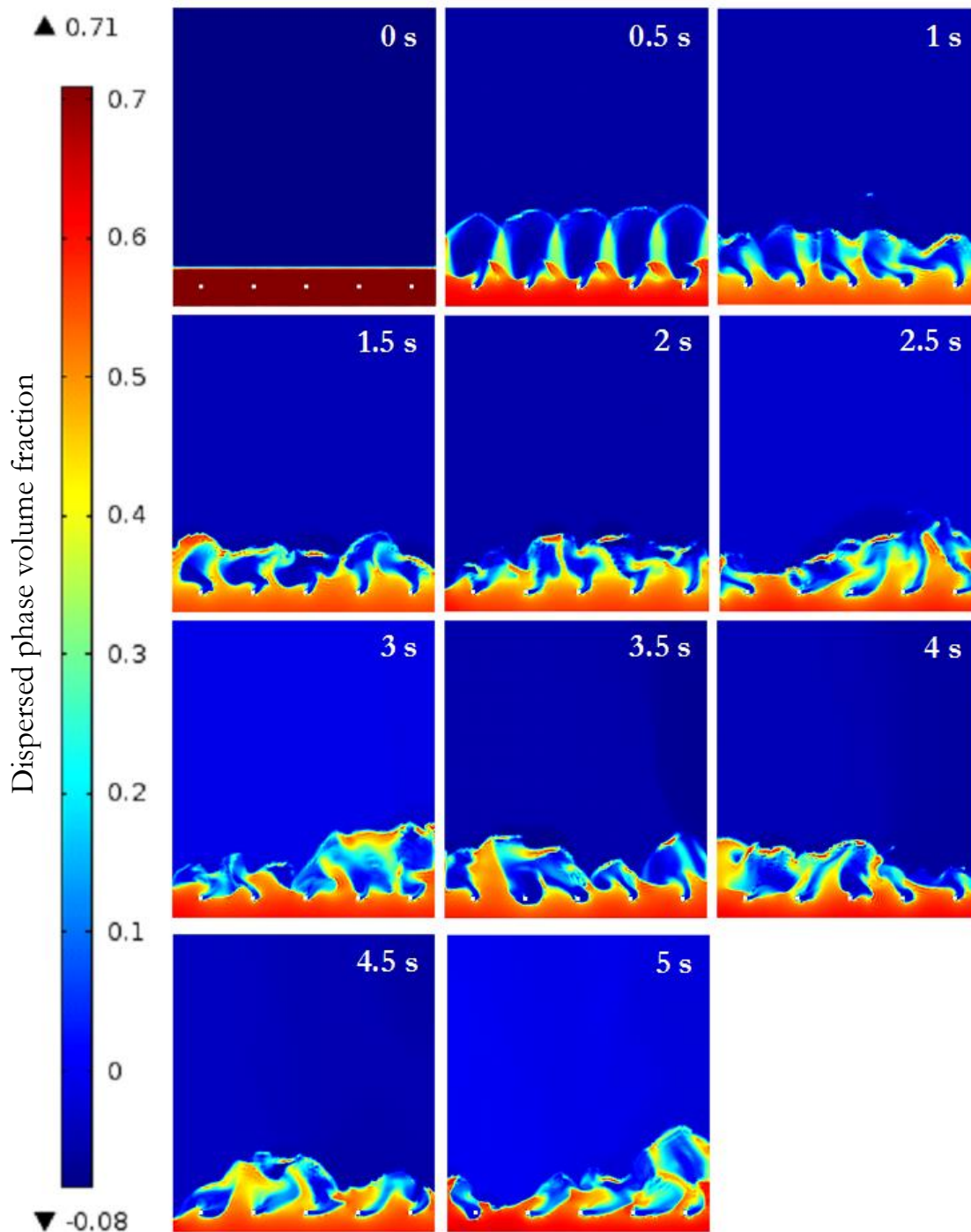


**Figure 6-2:** Instantaneous snapshots of simulation results (2.5 kg river sand; 6.5 mm tangential injectors)

One property that is not visibly obvious in the experiments conducted with the Perspex model is the dynamic viscosity of the dispersed phase, which relates to the resistance to flow and/or movement (refer to Chapter 5). In Figure 6-3, the yellow encircled areas located directly behind and below the air injectors indicate areas of high viscosity, whereas areas of low viscosity are illustrated in black and shades of red.

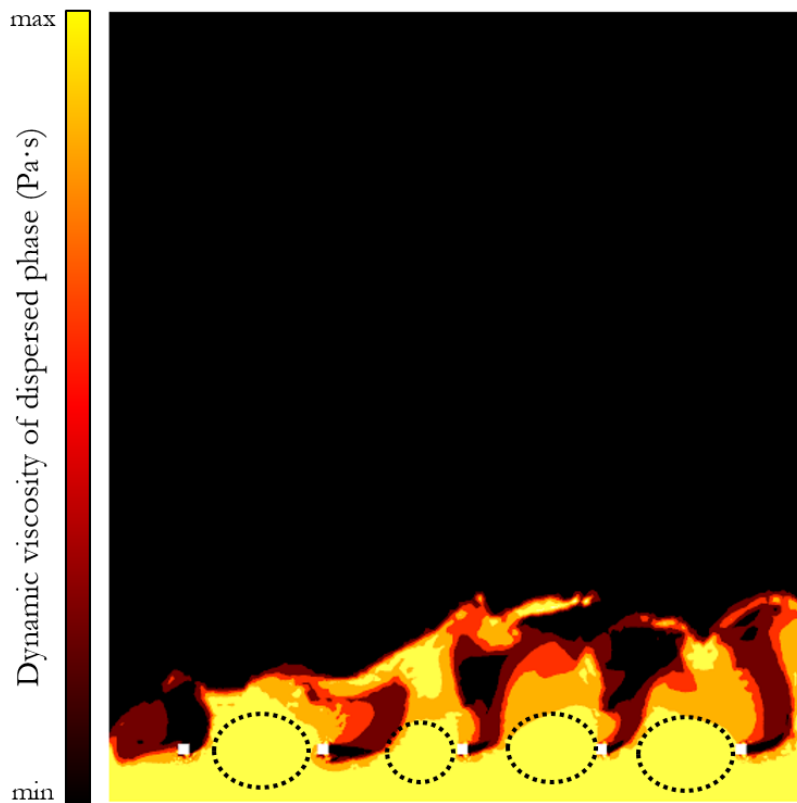


**Figure 6-3:** Dynamic viscosity of dispersed phase – encircled areas indicate areas of high dynamic viscosity (2.5 kg river sand; 6.5 mm tangential injectors)

The encircled areas in Figure 6-3 represent the stationary bed material located directly behind the injectors observed in the experiments conducted with the Perspex model (refer to Figure 6-2). As concluded in Chapter 4, it is these areas of stationary bed material, which have a high viscosity, that impede the momentum transfer between the moving air and river sand. As the air leaves the air injector, it encounters these areas of high viscosity that force the air vertically upwards, resulting in the formation of jets and spouted fluidized bed behaviour.



Similar results to those depicted in Figure 6-2 and Figure 6-3 were obtained for the remaining river sand loadings of 3.0 kg, 3.5 kg and 4.0 kg. A reduction in the air injector size, from 6.5 mm to 5 mm, and an increase in the superficial gas velocity, yielded comparable results to those described in Chapter 4.

### 6.2.2 Additional Materials

Simulating the ilmenite and the ilmenite-sand mixture proved to be problematic. In both cases, the simulations failed to solve even after a reduction in the simulation time and adjustments in the mesh element size. The failure to solve these simulations was likely due to several factors. The very small particle sizes of the dispersed phase (0.14 mm and 0.17 mm respectively), as well as the exceptionally large differences in density between the two phases (between 4 530 kg/m<sup>3</sup> and 3 690 kg/m<sup>3</sup>), made these simulations computationally intensive and subject to large errors in convergence.

Simulating the mustard seeds also proved to be problematic due to the large particle size of the individual seeds. In any case, the results of experiments conducted with the Perspex model using the mustard seeds proved to be uninteresting, with little bed expansion and only spouted fluidized bed behaviour being observed. For the reasons stated above, the simulation results obtained for the ilmenite, the ilmenite-sand mixture as well as the mustard seeds were omitted in this dissertation.

Figure 6-5 illustrates a series of instantaneous snapshots of the CFD model simulating 1.0 kg of poppy seeds over a period of 5 seconds using 5 mm tangential air injectors. The simulation results for poppy seeds depicted in Figure 6-5 compare well to the observed Perspex model results discussed in Chapter 4 (refer to Figure 4-11 (*top*)). Evidently, a pseudo-steady state is achieved within 1 second of commencing the simulation and the formation of jets and spouted fluidized bed behaviour was observed. As with the river sand simulations described previously,

stationary regions of bed material located directly behind the air injectors were apparent which impeded the momentum transfer between the moving air and the poppy seeds.

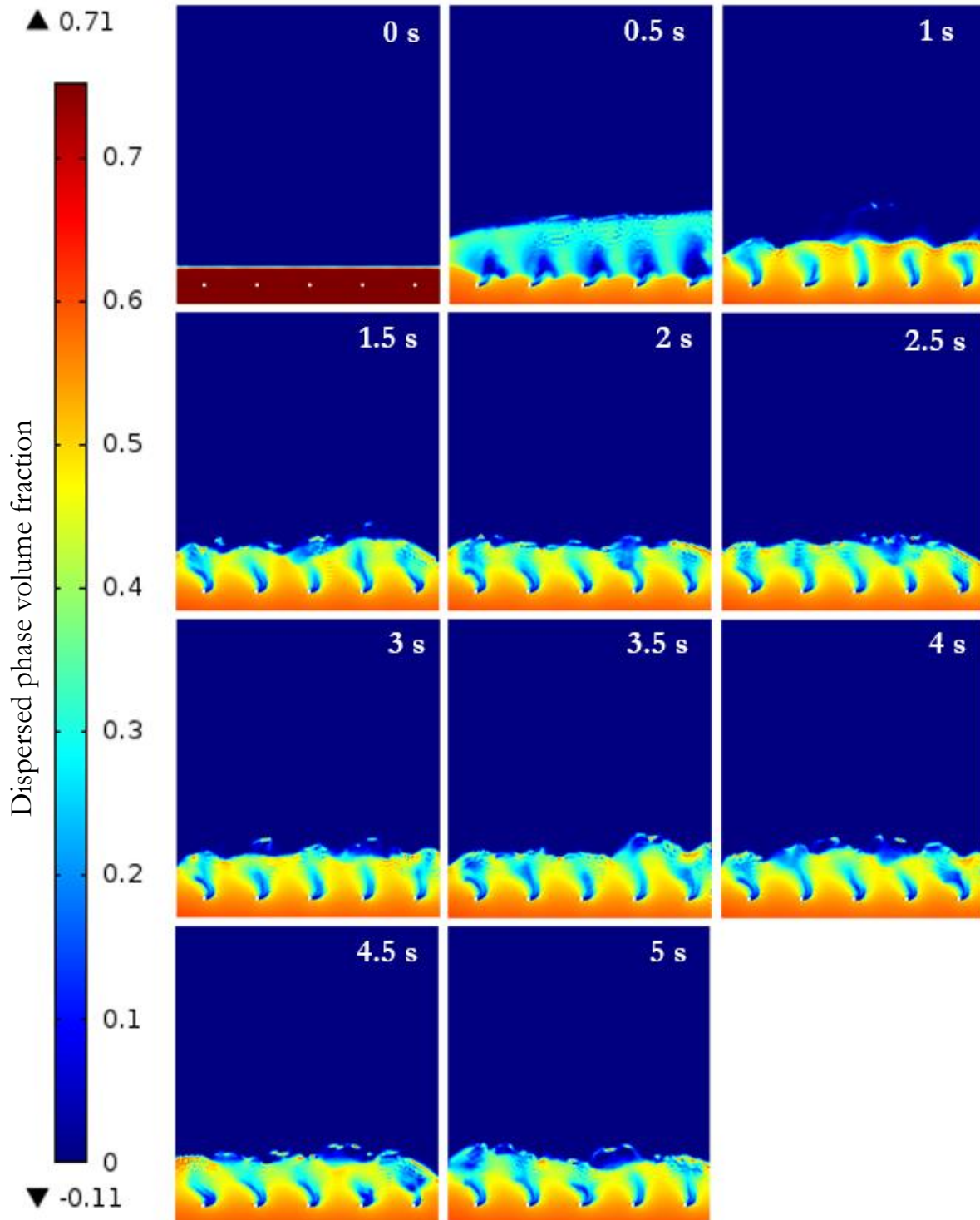


**Figure 6-4:** Instantaneous snapshots of simulation results (1.0 kg poppy seeds; 5 mm tangential air injectors)

## 6.3 Angled Blades

As with the simulations of the tangential air injectors described previously, only a section of the annulus was modelled on a 2D surface in order to reduce the computational time. Nine angled steps (inlH), representing nine overlapping metal leaves in the Perspex model, were equally spaced out along the bed width (bedW). The initial dispersed phase height (solidH0) varied depending on the bed simulated material loading, and an outlet boundary located at the top of the geometry at the bed height (bedH) allowed the rising air to escape. The same values for the above parameters were used as those listed in Table 6-1. However, inlH, which is the injector size in Table 6-1, was reduced to 0.5 mm to represent a slit height of 0.5 mm of the overlapping metal leaves.

The results for the 2.5 kg river sand loading are discussed in detail in the following section, and a general conclusion is drawn for the remaining river sand loadings. A brief discussion is also included on the poppy seed simulations using the CFD model of the angled blades.

### 6.3.1 River Sand

The material-specific parameters used in the 2.5 kg river sand loading simulation are the same as those listed in Table 6-2. The physics-controlled mesh generated for the geometry comprised 70 444 triangular elements and 1 485 quadrilateral elements. Significantly more elements were required to reach convergence with this geometry, because regions of mass imbalances were detected during initial simulations.

The simulation was studied over a period of 5 seconds to ensure sufficient time for the simulation to reach a pseudo-steady state. Figure 6-5 illustrates how the dispersed phase volume fraction changes over time in a series of instantaneous snapshots.

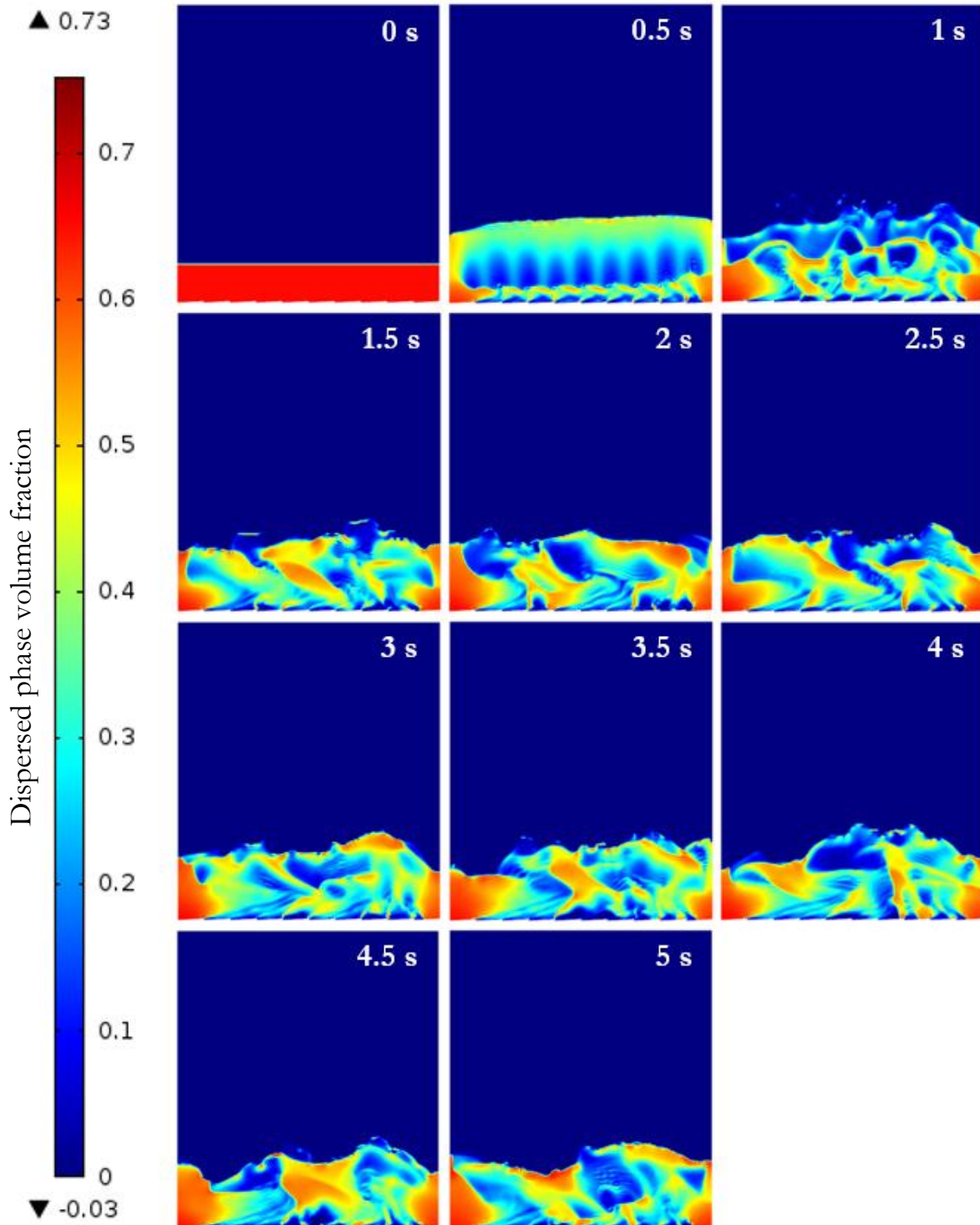


**Figure 6-5:** Instantaneous snapshots of simulation results (2.5 kg river sand; overlapping metal leaves)

The simulation results depicted in Figure 6-5 over-predict the bed expansion in comparison to the observed Perspex model results discussed in Chapter 5. In addition, it was mentioned in the previous chapter that at a superficial gas velocity

of 0.5 m/s in the annulus, the fluidized bed seemed to give the impression that it was rotating slightly in the opposite direction to the slits. It was then concluded that the fluidizing air was forming eddies as it impacted on the stationary bed material, pushing the fluidized air and fluidized bed material in the opposite direction. Interestingly, the results depicted in Figure 6-5 do not show any regions of stationary bed material located on top of the angled steps which remained the same size throughout the simulation period. In order to check for eddy formation, the velocity profile of the continuous phase was superimposed onto one of the instantaneous snapshots illustrated in Figure 6-5 to yield Figure 6-6. Proportional vectors of the continuous phase directed in the opposite direction to the slits (negative x-direction) near the bed surface are apparent, but regions of stationary bed material are not. The simulation results for the remaining river sand loadings of 3.0 kg, 3.5 kg and 4.0 kg were similar to those depicted in Figure 6-5 and Figure 6-6.

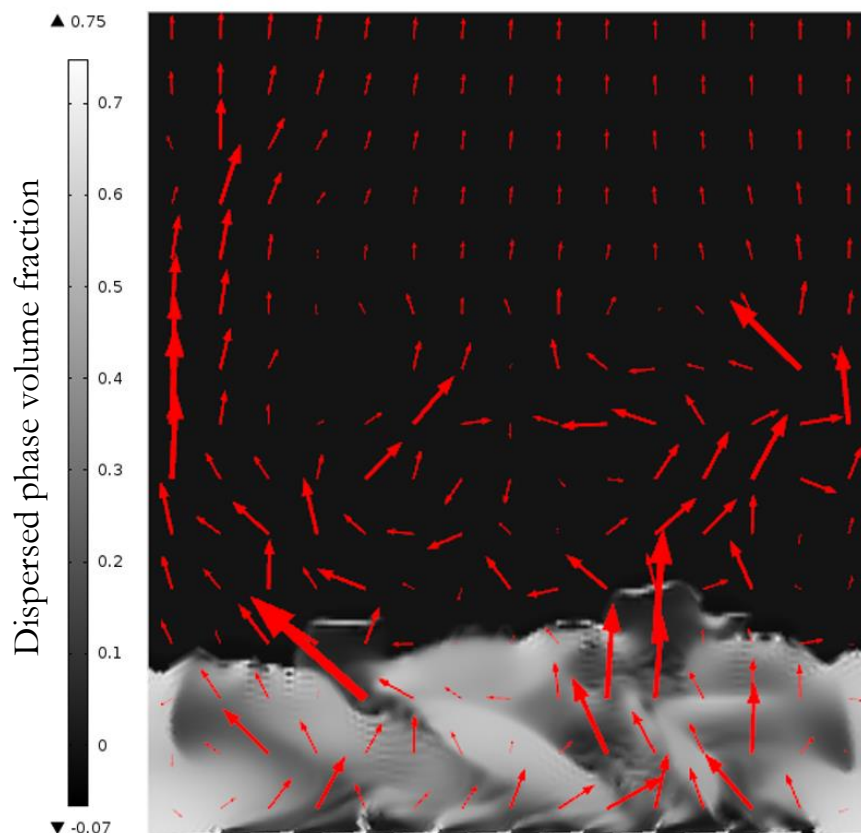


**Figure 6-6:** Velocity profile of continuous phase represented by proportional vectors at 1.5 seconds (2.5 kg river sand; overlapping metal leaves)



Simulating the 3D printed air distributor proved problematic and the simulation results were not comparable to those observed with the Perspex model. For all river sand loadings, the bed expansion was significantly over-predicted and large mass imbalances were observed. Even with a reduction in the simulation time and adjustments in the mesh element sizes and geometry, the simulations either failed to solve or resulted in large errors in convergence. It was therefore concluded that although it is possible to accurately duplicate the geometry of the physical Perspex model in a CFD model, small details in an overall large geometry, such as the slits in the 3D printed air distributor, are impractical to simulate and can lead to poor convergence.

### **6.3.2 Poppy Seeds**

The simulation results of the angled blades using poppy seeds as the bed material in the annulus were not comparable with those observed with the Perspex model. As with the simulation results of the angled blades using river sand, no regions of stationary bed material on top of the angled blades were observed. In addition, the formation of jets and spouted fluidized bed behaviour was also not observed. Instead, over the course of the simulation time, the bed of poppy seeds appeared to behave as a single expanding solid unit, significantly over-predicting the bed expansion. This observation was likely due to the fact that the particle size of the poppy seeds was larger than the mesh elements, resulting in many inaccuracies in the simulation and poor convergence.

Simulating the poppy seeds with the 3D printed air distributor also proved problematic due to large mass imbalances and the bed of poppy seeds behaving as a single expanding solid unit, as illustrated in Figure 6-7. Even with a reduction in the simulation time and adjustments in the mesh element sizes as well as geometry, the simulations failed to solve. Once again, the small details in an overall large geometry

were concluded to be impractical to simulate, ultimately leading to poor convergence.

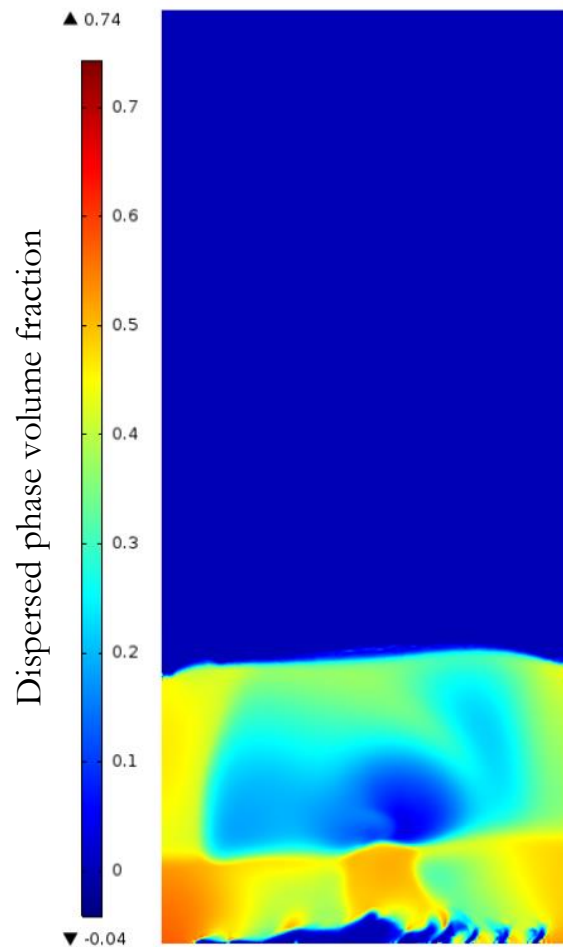


**Figure 6-7:** Instantaneous snapshot of simulation results (1.0 kg poppy seeds; 3D printed air distributor with 45° slits)

## 6.4 Limitations of CFD Results

Although CFD modelling offers many advantages over carrying out physical experiments, certain drawbacks are limiting to the applicability of the simulated results. Currently most CFD models, including the Euler-Euler Model used for the simulations in this chapter, model the dispersed phase as a single particle size. More accurate solutions could be achieved if the dispersed phase were modelled as a particle size distribution. Furthermore, 3-dimensional modelling of the annulus could also result in more accurate solutions. Finally, in Chapter 5 it was hypothesised



that once uniform fluidization is achieved in the annulus, induced rotating fluid bed behaviour is likely to occur with sufficient fluidizing air flowing in the tangential direction. In order to test this hypothesis, it is recommended that the annulus should be modelled at high Reynolds numbers in the turbulent regime. Several models are available for turbulent CFD modelling (Table 6-3); however, they are not currently available in COMSOL Multiphysics®. It is therefore recommended that more accurate solutions could be achieved if the dispersed phase is modelled as a particle size distribution, the annulus is modelled in three dimensions and a turbulent CFD model, capable of simulating high Reynolds numbers, is used.

## 6.5 Conclusions and Recommendations

The Euler-Euler Model – Laminar Flow Interface in COMSOL Multiphysics® was used to study the hydrodynamic behaviour of the annular fluidized bed in more detail. Although induced rotating fluid bed behaviour was not observed during any of the simulations, the results still proved beneficial since the CFD models could illustrate several hydrodynamic properties not visibly obvious in the experiments conducted with the Perspex model. The simulation results obtained for the ilmenite, the ilmenite-sand mixture and the mustard seeds were omitted in this dissertation due to failure to solve and large errors in convergence.

The simulation results of the tangential injectors with river sand and poppy seeds compared well to the observed Perspex model results, although over-prediction of bed expansion was observed. The simulation results supported the previously drawn conclusion that the areas of stationary bed material, which have a high viscosity, impede the momentum transfer, resulting in the formation of jets and spouted fluidized behaviour. The simulation results of the angled blades with river sand and poppy seeds, on the other hand, did not yield comparable results to those observed with the Perspex model as no stationary regions of bed material were observed on

top of the angled steps. It was concluded that although it is possible to create the geometry of the CFD model to very accurately represent the physical Perspex model, small details in an overall large geometry, such as the angled steps and slits, are impractical to simulate and can lead to poor convergence.

It is recommended that more accurate solutions could be achieved if the dispersed phase were modelled as a particle size distribution and the annulus were modelled in three dimensions. In addition, the annular fluidized bed should also be modelled using a turbulent CFD model capable of simulating high Reynolds numbers. Once the above suggestions have been implemented, the CFD models could then be used to test the recommendations suggested in Chapter 5, including porous plate-type distributors and variations in slit or hole angles with high superficial gas velocities in the annulus. If induced rotating fluid bed behaviour is successfully simulated, the CFD model could then be used to check whether sufficient contact time were available for the pyrolysis reactions to occur at those superficial gas velocities.

## 6.6 Reference

Silva, GG, Jiménez, NP and Salazar, OF (2012) *Fluid Dynamics of Gas-Solid Fluidized Beds*, In Oh, HW (ed) *Advanced Fluid Dynamics*, InTech.

**Table 6-3:** Summary of models suitable for turbulent CFD modelling (adapted from Silva, Jiménez & Salazar, 2012: 45)

| Family group and models  | Description and advantages   |
|--|--|
| <b>Reynolds-Averaged Navier-Stokes (RANS)</b><br>Zero equation models<br>One equation models<br>Two equations models such as $\kappa - \epsilon$ and $\kappa - \omega$ | The most widely used models. The main advantages are stable calculations, short computational times and reasonable results for many flows.   |
| <b>Reynolds Stress Model (RSM)</b>   | Provides good predictions for all types of flows including separation and swirling. Calculations times are longer than those of RANS models.   |
| <b>Large Eddy Simulation (LES)</b><br>Smagorinsky-Lilly model<br>Dynamic subgrid-scale model<br>RNG – LES model<br>WALLE model   | Provides excellent results for all types of flow. LES solves the Navier-Stokes equations for large-scale motions of the flow models.   |
| <b>Detached Eddy Simulation (DES)</b>  | Difficulties associated with the use of the standard LES models resulted in the development of hybrid models like that of DES. Attempts to combine the best aspects of RANS and LES methodologies in a single-solution strategy. |
| <b>Direct Numerical Simulation (DNS)</b>   | The most exact approach to turbulence simulation without requiring any additional modelling beyond the Navier-Stokes equations used to describe the turbulent flow regime.   |

---

# CHAPTER 7: CONCLUSIONS & RECOMMENDATIONS

---

A physical model was constructed using two Perspex tubes to study the behaviour of a fluidized bed in an annulus, testing various bed materials. In order to study the hydrodynamics of the annular fluidized bed in more detail, representative 2-dimensional CFD models were simulated in COMSOL Multiphysics® software. The conclusions and recommendations in Chapters 4, 5 and 6 are summarized below.

## 7.1 Perspex Model Conclusions

### 7.1.1 Tangential Injectors

It was hypothesized that by using multiple gas injectors orientated tangentially to the annulus walls, induced rotating fluid bed behaviour would occur in the annulus. Unfortunately, even after a reduction in the air injector diameter and the addition of a secondary blower, induced rotating fluid bed behaviour was not observed throughout the entire range of superficial gas velocities tested. Instead, as the superficial gas velocity increased beyond minimum fluidization, the formation of jets and spouted fluidized bed behaviour was observed, followed by turbulent fluidization. Regions of stationary bed material located directly behind the air injectors were also present for all materials tested. Based on these observations, it was concluded that the centrifugal forces were significantly lower than initially anticipated. Furthermore, it was concluded that the regions of stationary bed material, causing non-uniform fluidization, impede the momentum transfer between the moving air and bed material, preventing the possibility of any rotation of the bed material in the annulus.

### 7.1.2 Angled Blades

A completely different air distributing system was designed which may possibly have overcome the difficulties experienced with the multiple tangential air injectors. It was hypothesized that fixed angled blades, similar to the blades used in the gas distributor of the TORBED reactor, could induce a rotating fluid bed in an annulus. A metal air distributor was designed and manufactured from stainless steel with 32 overlapping metal leaves. Unfortunately, over the entire range of superficial gas velocities tested, and with various slit heights, induced rotating fluid bed behaviour was not observed for any of the materials tested. Jet formation and spouted fluidized bed behaviour was again observed as the superficial gas velocity was gradually increased, followed by turbulent fluidization. Stationary regions of bed material, located on top of the overlapping metal leaves, were also observed but were significantly smaller in size compared to the regions observed directly behind the tangential air injectors. Based on these observations, it was concluded that the vertical and tangential components ( $v \sin\theta$  and  $v \cos\theta$ ) of the air velocity flowing through the overlapping metal leaves were insufficient to result in uniform fluidization or the desired induced rotating bed behaviour in the annulus.

In order to overcome the problems experienced with the metal air distributor, a new 3D printed air distributor was designed to have 64 slits with fixed slit heights of 0.5 mm at an angle of  $45^\circ$ . Although induced rotating fluid bed behaviour was once again not observed with any of the materials tested at any superficial gas velocity, uniform bubbling fluidization was observed during experiments conducted with river sand and poppy seeds. This observation implied that the vertical component ( $v \sin\theta$ ) of the velocity flowing through the slits was sufficient to achieve uniform fluidization in the annulus, significantly increasing the mixing effects of the bed material. However, the tangential component ( $v \cos\theta$ ) of the velocity was still insufficient to induce any rotation of the fluid bed in the annulus.

From independent research conducted at the Pyrolysis Laboratories in the Department of Chemical Engineering at the University of Pretoria, it was concluded that the regions of stationary bed material previously described had a high viscosity and therefore a high resistance to flow and/or movement. As the fluidizing air impacted on these regions of high viscosity, the moving air was forced vertically upwards, resulting in the formation of jets and spouted fluidized bed behaviour.

## 7.2 Conclusions of CFD Simulations

The Euler-Euler Model – Laminar Flow Interface in COMSOL Multiphysics® software was used to study the hydrodynamic behaviour of the annular fluidized bed in more detail. Although induced rotating fluid bed behaviour was not observed during any of the simulations, the results still proved beneficial since the CFD models could illustrate several hydrodynamic properties not visibly obvious in the experiments conducted with the Perspex model.

The simulation results of the tangential injectors with river sand and poppy seeds compared well to the observed Perspex model results, although slight over-prediction of bed expansion was apparent. The simulation results supported the previously drawn conclusion that the areas of stationary bed material, which had a high viscosity, impeded the momentum transfer and resulted in the formation of jets and spouted fluidized behaviour. The simulation results of the angled blades with river sand and poppy seeds on the other hand, did not yield comparable results to those observed with the Perspex model as no stationary regions of bed material were observed, and neither was uniform bubbling fluidization. It was therefore concluded that although it is possible to create the geometry of the CFD model to very accurately represent the physical Perspex model, small details in an overall large geometry, such as the angled steps and slits, are impractical to simulate and can lead to poor convergence.

### 7.3 Recommendations for Future Work

After the analysis of all the experimental work performed, it was hypothesized that once uniform fluidization is achieved, induced rotating fluid bed behaviour is likely to occur with sufficient fluidizing air flowing in the tangential direction since a uniformly fluidized bed offers little resistance to flow and/or movement. It is recommended that future experiments should be conducted using slit (or hole) angles below  $45^\circ$  and with blowers able to achieve higher superficial gas velocities in the annulus ( $>1$  m/s). Future experiments should also test porous plate-type air distributors which, if manufactured from ceramic materials, would also be more practical for the annular pyrolysis chamber in the new fluidized bed fast pyrolyser.

In the event that more accurate CFD models of the annular fluidized bed were developed, it is recommended that the dispersed phase should be modelled as a particle size distribution and the annulus modelled 3-dimensionally. In addition, the annular fluidized bed should also be modelled using a turbulent CFD model capable of simulating high Reynolds numbers. If induced rotating fluid bed behaviour were successfully modelled using CFD, the model could then be used to check whether sufficient contact time were available for the pyrolysis reactions to occur at those superficial gas velocities. If not, the design concept of an induced rotating fluid bed in the annular pyrolysis chamber of the new fluidized bed fast pyrolyser would be impractical. In such an event, a rotating gas distributor plate should be considered instead.